Circulation

ORIGINAL RESEARCH ARTICLE

Integrative Molecular Analyses of Inflammatory and Autoimmune Signals in Cardiac Sarcoidosis

Meraj Neyazi, MD*; Gabriela Venturini, PhD*; Kemar J. Brown, MD; Youjung Choi, MD, PhD; Joshua M. Gorham, BA; Olivia G. Layton, BA; Arjun Verma, BA; Adam J. Wang, BA; Ryan T. Gross, BS; Barbara A. McDonough, RN; Michelle Mendiola Pla, MD, MHS; Anissa Viveiros, MsC, PhD; Daniel M. DeLaughter, PhD; Steven R. DePalma, PhD; Yuri Kim, MD, PhD; Daniel Reichart, MD; Hiroko Wakimoto, MD, PhD; Stephen J. Elledge, PhD; Sanjay Divakaran, MD; Richard N. Mitchell, MD, PhD; Jiwon Koh, MD, PhD; Jun-Bean Park, MD, PhD; Dawn E. Bowles, PhD; Carolyn Glass, MD, PhD; Gavin Y. Oudit, MD, PhD; Jonathan G. Seidman, PhD*; Christine E. Seidman, MD*

BACKGROUND: Cardiac sarcoidosis (CS) is an enigmatic disorder characterized by unexplained patchy, sterile granulomas intermixed with preserved myocardium and fibrotic regions without granuloma. CS causes arrhythmias, sudden cardiac death, and heart failure. The mechanisms producing this remarkable histopathology and disease progression remain unexplained.

METHODS: Using comprehensive single-cell and spatial transcriptomic analyses, we characterized the cellular composition and gene expression in preserved, granulomatous, and fibrotic regions of human CS hearts. From unexpectedly identified clonally expanded cardiac B cells with rearranged immunoglobulin sequences, we reconstructed antibodies and screened libraries comprising the human peptidome or microbial and allergen peptides to define reactive epitopes in CS hearts.

RESULTS: Cellular composition and gene expression differed substantially in CS tissues with preserved, granulomatous, or fibrotic histopathology. Cardiomyocytes upregulated arrhythmogenic and inflammasome transcripts associated with pyroptosis. Cardiomyocytes and fibroblasts activated chemoattractant cytokines that sustained myeloid and lymphoid infiltration. Granulomas contained abundant macrophages expressing modulators of cell–cell fusion, along with Th17-skewed T cells that upregulated B-cell–activating factor, thereby promoting antibody production. Fibrotic regions, without active granulomas, exhibited tertiary lymphoid structures, with clonal expansion of mature B and plasma cells. Reconstructed antibodies derived from expanded B-cell clones were inert to microbial and allergen peptides, but reacted to PPL (periplakin), a desmosome protein, and other peptides expressed on cardiac cells.

CONCLUSIONS: Progressive inflammatory signals in CS are mediated by chemoattractant genes in cardiomyocytes and fibroblasts within preserved myocardium, cell–cell fusion modulators in activated macrophages within granulomatous regions, and tertiary lymphoid structures in fibrotic regions that produce patient-specific autoimmune antibodies. Identification of PPL as a CS autoantigen may account for shared clinical manifestations in CS and arrhythmic desmosomal cardiomyopathies. CS autoantigens may underlie enigmatic histopathologic findings, perpetuate disease, and contribute to adverse outcomes. Uncovering an intracardiac humoral autoimmune axis in CS provides specific therapeutic opportunities to limit granuloma formation and B-cell activation, which may reduce arrhythmogenicity and progressive dysfunction. Parallel analytic strategies have potential to define autoantigens in other enigmatic cardiac immune disorders.

Key Words: autoantibodies ■ cardiomyopathies ■ inflammation ■ sarcoidosis ■ sequence analysis, RNA ■ spatial transcriptomics

Correspondence to: Christine E. Seidman, MD, Cardiovascular Division, Brigham and Womens Hospital, 77 Avenue Louis Pasteur, Boston, MA 02186. Email cseidman@genetics.med.harvard.edu

*M. Neyazi, G. Venturini, J.G. Seidman, and C.E. Seidman contributed equally.

Supplemental Material is available at https://www.ahajournals.org/doi/suppl/10.1161/CIRCULATIONAHA.126.079304.

Circulation is available at www.ahajournals.org/journal/circ

ORIGINAL RESEARCH ARTICLE

Clinical Perspective

What Is New?

- Discrete histopathologic regions in cardiac sarcoidosis (CS) tissues—preserved, granulomatous, and fibrotic—exhibit spatially distinct cellular compositions and molecular signatures.
- Granulomas, the hallmark of CS, reflect dysregulated levels of specialized immune cells with macrophages that express genes for cellular fusion and inflammation or genes regulating tissue repair.
- Clonal expansion of intramyocardial B cells in CS can produce autoantibodies that perpetuate histopathology and promote disease progression.

What Are the Clinical Implications?

- The patchy distribution of histopathology in CS tissues belies profound molecular changes within preserved, granulomatous, and fibrotic regions that allow disease to resolve, smolder, or progress to heart failure.
- Inflammatory signals and autoimmune antibodies in CS mimic processes identified in arrhythmic cardiomyopathies, accounting for shared clinical manifestations in these disorders.
- Molecular signals activated in distinct histopathologic regions of CS indicate therapeutic targets that may allow precision medicines to limit inflammation, autoimmunity, and disease progression.

Nonstandard Abbreviations and Acronyms

BAFF	B-cell activating factor
CDR3	complementary-determining region 3
CHI3L1	chitinase-3-like protein 1
CS	cardiac sarcoidosis
DCM	dilated cardiomyopathy
ECM	extracellular matrix
ERC1	ELKS/Rab6-interacting/CAST family member 1
gp39	glycoprotein-39
GRIK2	glutamate ionotropic receptor kainate type subunit 2
HF	heart failure
IFN-γ	interferon-γ
IL-1	interleukin-1
IL-16	interleukin-16
IVS	interventricular septum
LV	left ventricular
LVFW	left ventricular free wall
mTORC1	mammalian target of rapamycin complex 1
NRXN1	neurexin-1
PhIP-seq	profiled duplicate phage immunoprecipitation sequencing
PPL	periplakin
snRNA-seq	single nucleus RNA sequencing
SPATA7	spermatogenesis-associated 7
SPECC1L	sperm antigen with calponin homology and coiled-coil domains 1-like
TLS	tertiary lymphoid structures
USP5	ubiquitin-specific protease 5
V(D)J	variable–(diversity)–joining

Granulomas, the diagnostic hallmark of sarcoidosis, randomly appear in tissues, resolve, and reappear in the same or other organs—a scenario that incites acute flares and smoldering chronic dysfunction.[1] Cardiac sarcoidosis (CS), with particularly insidious onset and patchy tissue involvement, accounts for most sarcoidosis-related deaths,[2–4] and exhibits suboptimal responses to therapeutic immunosuppression,[5] cardiac medications, and anti-arrhythmic devices[6]—none of which prevents disease progression.

We analyzed 41 heterogenous CS ventricular tissues using single nucleus RNA sequencing (snRNA-seq) to define regional cell type composition and molecular properties in comparison with normal and dilated cardiomyopathy (DCM) hearts.[7,8] By incorporating spatial transcriptomics, we anchored molecular profiles within intact CS tissues to link cellular location with regional inflammatory signals. We captured B- and T-cell variable–(diversity)–joining (V[D]J) sequences and defined clonal amplification and functional states of lymphocytes. Using B-cell receptor sequences, we reconstructed tissue-derived antibodies, screened phage-display libraries comprising the human peptidome or microbial and allergen peptides,[9,10] and uncovered antigenic targets. The resultant high-resolution CS cell atlas revealed distinguishing features for preserved, granulomatous, and fibrotic regions and uncovered a humoral autoimmune axis and cellular responses that promoted damage and disease progression. We nominate molecular circuits and therapies that target specific components of this enigmatic disorder.

METHODS

Detailed descriptions of approaches and technologies are provided in the Supplemental Methods and summarized here.

Study Population

Patients with CS provided written informed consent for deidentified tissue acquisition, using protocols reviewed and approved by participating institutions. Table S1 provides clinical data of the patients with CS, previously reported healthy heart donors,[7] and patients with DCM.[8]

Circulation. 2026;153:2011–2028. DOI: 10.1161/CIRCULATIONAHA.126.079304

Sample Categorization and Processing for snRNA-seq

Ventricular tissues were obtained during mechanical circulatory support implantation, heart transplantation, autopsy, or septal myectomy. CS was diagnosed by board-certified academic cardiovascular pathologists with expertise in sarcoidosis. Histopathology enabled categorization of individual tissue sections (Table S2) as predominantly preserved, granulomatous, or fibrotic. Samples were processed for snRNA-seq, quality control filtered, and harmonized as described[7,8] (see Supplemental Methods).

Lymphocyte and V(D)J Analysis

B- and T-cell receptor sequences within Cell Ranger BAM files were analyzed using TRUST4[11] to reconstruct rearranged V(D)J sequences. Recovered nuclei, expressing antigen receptors and excluded by snRNA-seq quality control filters, were reintegrated, and all lymphocytes were analyzed together. Clonality was assessed by V(D)J junction sequences (see Supplemental Methods).

Phage Immunoprecipitation Sequencing

We synthesized recombinant antibodies corresponding to B-cell clones and, together with commercial control antibodies (Table S7 and Supplemental Methods), profiled duplicate phage immunoprecipitation sequencing (PhIP-seq) libraries comprising overlapping human peptides encompassing the peptidome or microbial and allergen peptides.[9,10] Reactivity of the PPL (periplakin) autoantibody, representing other autoantibodies, was confirmed by immunoprecipitation analyses.

Spatial Transcriptomics

Spatial transcriptomic profiling (10× Genomics Xenium platform) of fresh-frozen and archival formalin-fixed, paraffin-embedded tissues was analyzed using the Human Multi-Tissue and Cancer Gene Panel supplemented with 100 custom genes (Table S5). Data were integrated onto adjacent hematoxylin & eosin–stained sections.

Statistical Analysis

Bioinformatic analyses were performed using R Statistical Software (v4.4.0, R Core Team 2021) and Seurat v5.[12] Cell type and state abundance were assessed using centered log-ratio transformation before linear modeling and marker genes identified by the Wilcoxon rank-sum test. Differential gene expression (false discovery rate <0.05) for pseudo-bulk data was analyzed using the quasi-likelihood framework in edgeR v4.[13] Hypergeometric testing assessed Gene Ontology enrichment using clusterProfiler[14] and T- and B-cell clonotype size distributions. Multiple testing was corrected using the Benjamini-Hochberg method. Data are presented as mean±SEM unless stated otherwise.

Data and Materials Availability

CS snRNA-seq and spatial transcriptomic data sets are available in Gene Expression Omnibus under accession numbers GSE319770 and GSE319771, respectively. Published control and DCM snRNA-seq data[7,8] were deposited in the European Genome–Phenome Archive (accession number EGAS00001006374). The custom code used in this article is available at https://github.com/mneyazi/cardiac_sarcoidosis.

RESULTS

Study Cohort

Cardiac tissues from 22 patients with CS (55% with extracardiac involvement) were obtained from the left ventricular free wall (LVFW; n=21), left ventricular (LV) apex (n=6), LV interventricular septum (IVS; n=7), and right ventricular free wall (n=7; Figure 1A and Tables S1 and S2) during ventricular assist device placement (n=7), cardiac transplantation (n=13), myectomy (n=1), or autopsy (n=1). Self-reported ancestries were African (n=10), Northern European (n=10), or Asian (n=2). LV ejection fraction was <35% in 18 patients with CS. Seven patients received immunosuppression before tissue collection (Table S1). Although microbial infections may trigger sarcoidosis,[1] genome sequences from 9 patients with CS (Table S2) excluded bacterial, viral, or fungal sequences (Supplemental Methods).

Cellular Compositional Changes in CS Hearts

Based on predominant histopathologic findings (Figure 1B and 1C) and confirmed by cellular composition analyses of snRNA-seq data, we classified 41 CS tissues as preserved (normal myocardial architecture), granulomatous (prominent multinucleated giant cells), or fibrotic (reduced cellularity, prominent collagen-rich extracellular matrix [ECM]; Figure S2). Among 9 CS hearts with multiple samples, 5 had heterogeneous histopathologies and 4 were uniform, including 1 with preserved architecture (Table S2).

From tissue immediately adjacent to the classified histopathologic sections, we isolated and processed nuclei for snRNA-seq (Supplemental Methods). Using Harmony,[15] we integrated snRNA-seq data from CS, 12 nonfailing donor hearts (15 LVFW, 9 right ventricular free wall, 7 IVS), and 29 DCM hearts (27 LVFW, 21 right ventricular free wall, 18 IVS),[8] processed using identical protocols (Figure 1A). The final data set contained 584 906 nuclei, including 185 893 CS nuclei from preserved (n=54 177), granulomatous (n=30 912), and fibrotic (n=100 804) regions; 133 336 control nuclei; and 265 677 DCM nuclei (Figure 1D).

Ventricular tissues contained 10 major cell types: cardiomyocytes; fibroblasts; lymphoid, myeloid, neuronal, endothelial, smooth muscle, and mast cells; adipocytes; and pericytes (Figure 1D). Cell type proportions (Figure 1E and Figure S3) indicated that disease depleted cardiomyocyte abundances, with the greatest loss in CS (47.7%±2.5% versus CS 23.2%±2.7% [*P*=5.8e-6]). CS,

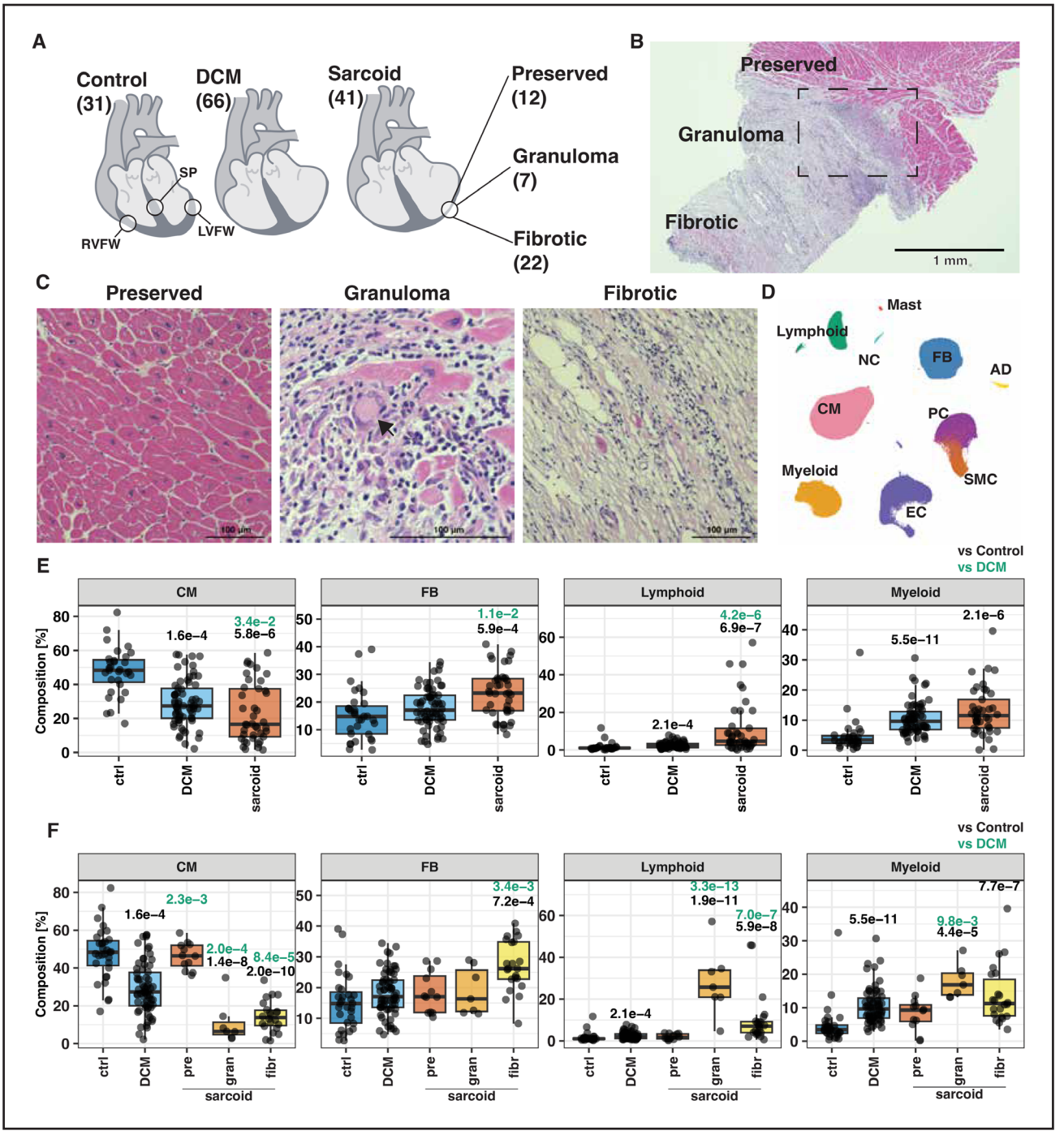

Figure 1. Variation in the cellular composition of 3 cardiac sarcoidosis regions.
A, Representation of ventricular tissues sampled from control, dilated cardiomyopathy (DCM), and sarcoid hearts (cardiac sarcoidosis [CS]). Samples were taken from the left ventricular free wall (LVFW), interventricular septum (SP), and right ventricular free wall (RVFW). **B**, Hematoxylin & eosin–stained sections from a CS heart demonstrating patchy histopathology with preserved, granulomatous (delineated by dashed outline), and fibrotic regions. **C**, Higher magnification of the tissue presented in **B** demonstrating cellular features of preserved (normal cardiac architecture), granulomatous (multinucleated giant cell [arrowhead] and immune cells), and fibrotic (reduced cellularity and increased extracellular matrix) regions. **D**, Uniform manifold approximation and projection embedding of nuclei obtained from control, DCM, and CS tissues characterized by single nucleus RNA sequencing identified 10 cell types. **E**, Proportional abundances of cell types that differed among control (ctrl), DCM, and CS tissues. Benjamini-Hochberg–adjusted *P* values (false discovery rate ≤0.05) for each test condition relative to controls (black) and DCM (green) are shown. **F**, Proportional abundances of cell types that differed among control, DCM, and sarcoid tissues, stratified as preserved (pre), granulomatous (gran), or fibrotic (fibr) by histopathology. Benjamini-Hochberg–adjusted *P* values (false discovery rate ≤0.05) for each test condition relative to controls (black) and DCM (green) are shown. AD indicates adipocytes; CM, cardiomyocytes; EC, endothelial cells; FB, fibroblasts; NC, neuron cells; PC, pericytes; and SMC, smooth muscle cells.

 Circulation. 2026;153:2011–2028. DOI: 10.1161/CIRCULATIONAHA.126.079304

unlike DCM, significantly expanded fibroblasts (mean CS, 23.1%±1.4%; mean control, 15.2%±1.6% [*P*=5.9e-4]). Immune cell population abundances varied considerably in CS, reflecting heterogeneous histopathology, with 6.4-fold more lymphocytes (10.9%±2.2% versus 1.7%±0.4% [*P*=6.9e-7]) and 2.7-fold more myeloid cells (13.0%±1.2% versus 4.8%±1.0% [*P*=2.1e-6]) than controls. Correlation analyses of cell type proportions showed that CS hearts lacked the reciprocal relationship between cardiomyocytes and fibroblasts found in control hearts and identified a strong negative correlation (more pronounced than in DCM) between lymphoid and cardiomyocyte populations (Figure S4).

Region-stratified cell type proportions (Figure 1C and Figure S5) showed considerable similarities for preserved CS and control tissues, with cardiomyocytes comprising almost 50% of all nuclei. By contrast, CS granulomatous tissues had 4.3-fold fewer cardiomyocytes (10.9%±4.3% [*P*=1.4e-8]), 17-fold more lymphoid cells (28.1%±6.1%; control, 1.7%±0.4% [*P*=1.9e-11]), and 3.7-fold more myeloid cells (17.9%±1.9%; control, 4.8%±1.0% [*P*=4.5e-5]). Fibrotic CS was similarly cardiomyocyte-depleted compared with control (14.4%±1.7% [*P*=2e-10]) and DCM (*P*=8.4e-5) tissues and showed fibroblast enrichment (27.0%±1.8% versus 15.2%±1.6% in controls [*P*=7.2e-4] and 18.0%±0.9% in DCM [*P*=3.4e-3]). In comparison with granulomatous tissue, fibrotic CS had smaller proportional increases in lymphoid cells (10.3%±2.6% [*P*=5.9e-8]) but maintained an increased abundance of myeloid cells (13.8%±1.9% [*P*=7.7e-7]).

We considered whether cardiac function correlated with histopathologic classifications or cell abundances, recognizing several limitations (ie, a small study cohort, few patients with normal cardiac function, variable treatment profiles and outcomes, regional tissue analyses rather than complete myocardial analyses). Immunosuppressive therapy (15 of 22 patients with CS), confounded by heterogeneity in regimen, duration, and timing relative to tissue sampling, had no substantive impact on cell type composition in preserved, fibrotic, or granulomatous regions or on differential gene expression in cardiomyocytes, fibroblasts, or myeloid or lymphoid cell populations (Tables S1, S2, and S4 and Figure S6). Systolic function, which was depressed in 17 of 22 patients, and ventricular tachycardia or fibrillation, which was documented in 13 patients and absent in 9 patients, showed no significant associations with regional histopathology or transcriptional changes (Tables S1 and S2 and Figure S8).

Spatial Transcriptomics Reveals Distinct Cellular Neighborhoods

We assessed tissue microenvironments in 8 control and 10 CS (5 granulomatous and fibrotic) samples using spatial transcriptomics, probed using a multitissue plus custom genes panel (Figure 2A and 2C, Supplemental Methods, and Table S5). Three spatially distinct neighborhoods were identified with enriched proportions of cardiomyocytes, immune cells, or fibroblasts (Figure 2D–2F). Control tissues contained almost exclusively (≈90%) cardiomyocyte neighborhoods. Because preserved CS closely resembled control myocardium, we presumed that cardiomyocyte neighborhoods predominated in preserved CS tissues. Cardiomyocyte neighborhoods were reduced in granulomatous and fibrotic CS tissues (Figure 2H) and contained fewer cardiomyocytes and more fibroblasts and immune cells than cardiomyocyte neighborhoods from control tissues (Figure 2I). Immune neighborhoods were markedly increased in granulomatous and fibrotic CS tissues, with higher lymphoid and myeloid cell abundances, suggesting disease-specific inflammatory microenvironments rather than physiologic immune infiltration. By contrast, fibroblast neighborhoods, rare in control and highest in CS fibrotic tissues, had similar cellular compositions across groups.

Sarcoidosis Drives Inflammatory and Electrophysiologic Gene Transcriptional Remodeling in Ventricular Cardiomyocytes

We analyzed transcriptional changes across key cell types to discern molecular signals vital to the neighborhood differences in CS regions. The abundances of previously characterized cardiomyocyte transcriptional states (ventricular cardiomyocytes)[8] were modestly different between CS stratified by tissue histopathology and controls (Figure 3A and B and Figure S7). However, differential gene expression revealed notable changes (Table S6).

Across all CS regions, cardiomyocytes upregulated genes encoding for E3 ubiquitin protein ligases (*HECTD1*, *HECTD2*, *HECTD4*[16]) and downregulated genes involved in ATP production (eg, NADH dehydrogenase subunit, cytochrome c oxidase subunits[17]). Such abnormalities in preserved CS inferred heightened protein ubiquitination and compromised energetics predated sarcoid histopathology.

In granulomatous and fibrotic regions, cardiomyocytes downregulated *FOXO3B*, a transcriptional modulator of autophagy or cell death, and *CSRP3*, encoding a muscle-specific LIM protein involved in force transmission and autophagy. Pathogenic variants in *CSRP3* cause DCM and reduced expression accompanies heart failure (HF).[18]

Cardiomyocytes in preserved, granulomatous, and fibrotic regions progressively dysregulated expression of cardiac electrophysiologic genes (Figure 3C), including downregulation of *CALM2* and *PERP*. *CALM2* encodes a modulator of calcium-calmodulin-dependent channels and kinases and pathogenic variants cause life-threatening arrhythmias.[19] *PERP* encodes a desmosome

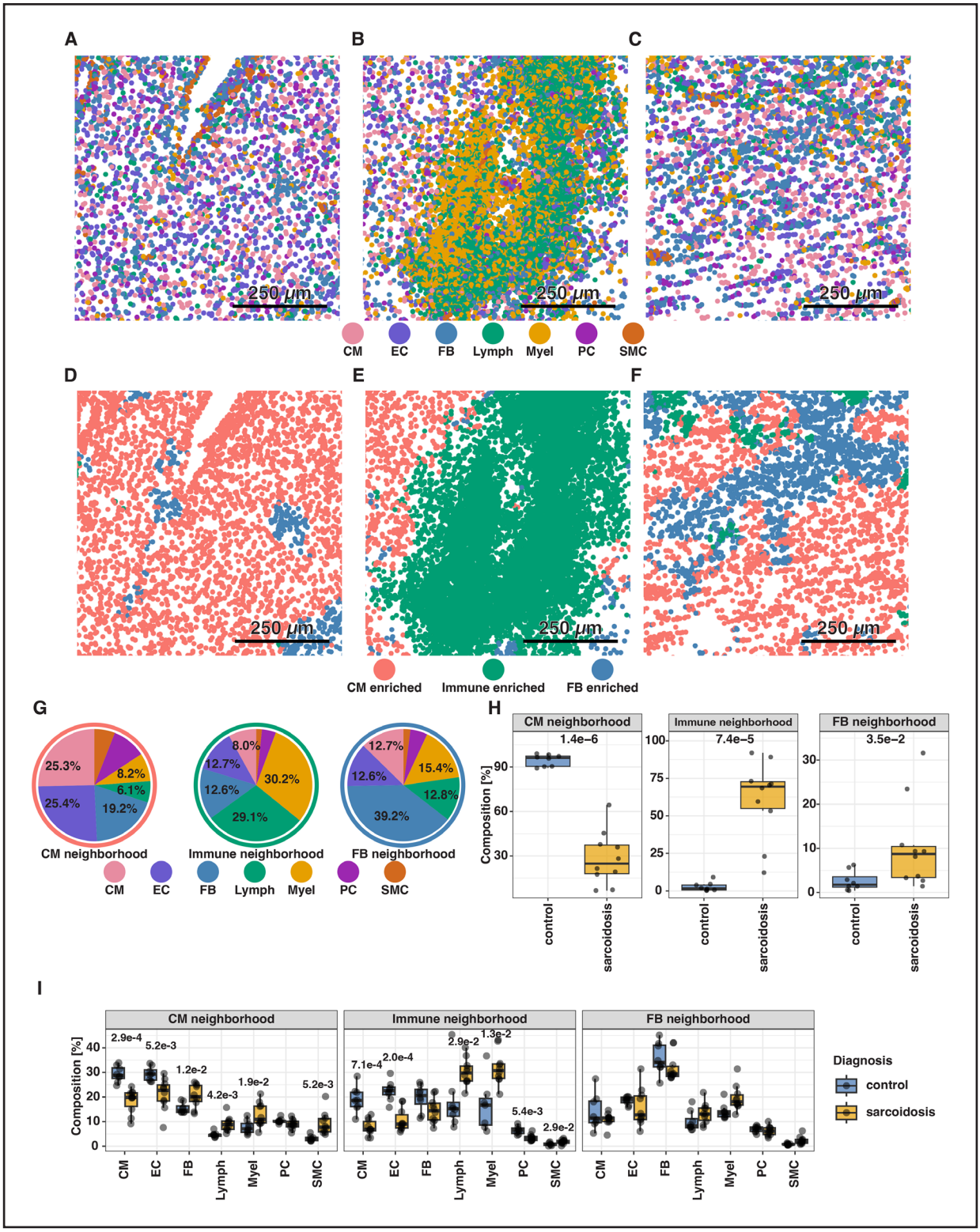

Figure 2. Spatial transcriptomics delineates distinct cellular neighborhoods in cardiac sarcoidosis tissues.
A through **C**, Spatial transcriptomics analyses of cardiac sarcoidosis tissues classified as preserved (**A**), granulomatous (**B**), and fibrotic (**C**). Colors denote cell types, inferred by expression of marker genes. **D** through **F**, Spatial defined neighborhoods (denoted by colors) from tissues shown in panels **A** through **C** were enriched for cardiomyocytes (CMs), immune cells (lymphoid [Lymph] and myeloid [Myel]), or fibroblasts (FBs). **G**, Pie charts summarizing cell-type compositions within each neighborhood. **H**, Comparisons of the prevalence of each neighborhood in control and sarcoidosis samples. Benjamini-Hochberg–adjusted *P* values from *t* tests displayed when false discovery rate ≤0.05. **I**, Comparisons of the cell type composition within spatial neighborhoods between control and cardiac sarcoidosis tissues. Benjamini-Hochberg–adjusted *P* values from *t* tests displayed when false discovery rate ≤0.05. EC indicates endothelial cells; PC, pericytes; and SMC, smooth muscle cells.

 Circulation. 2026;153:2011–2028. DOI: 10.1161/CIRCULATIONAHA.126.079304

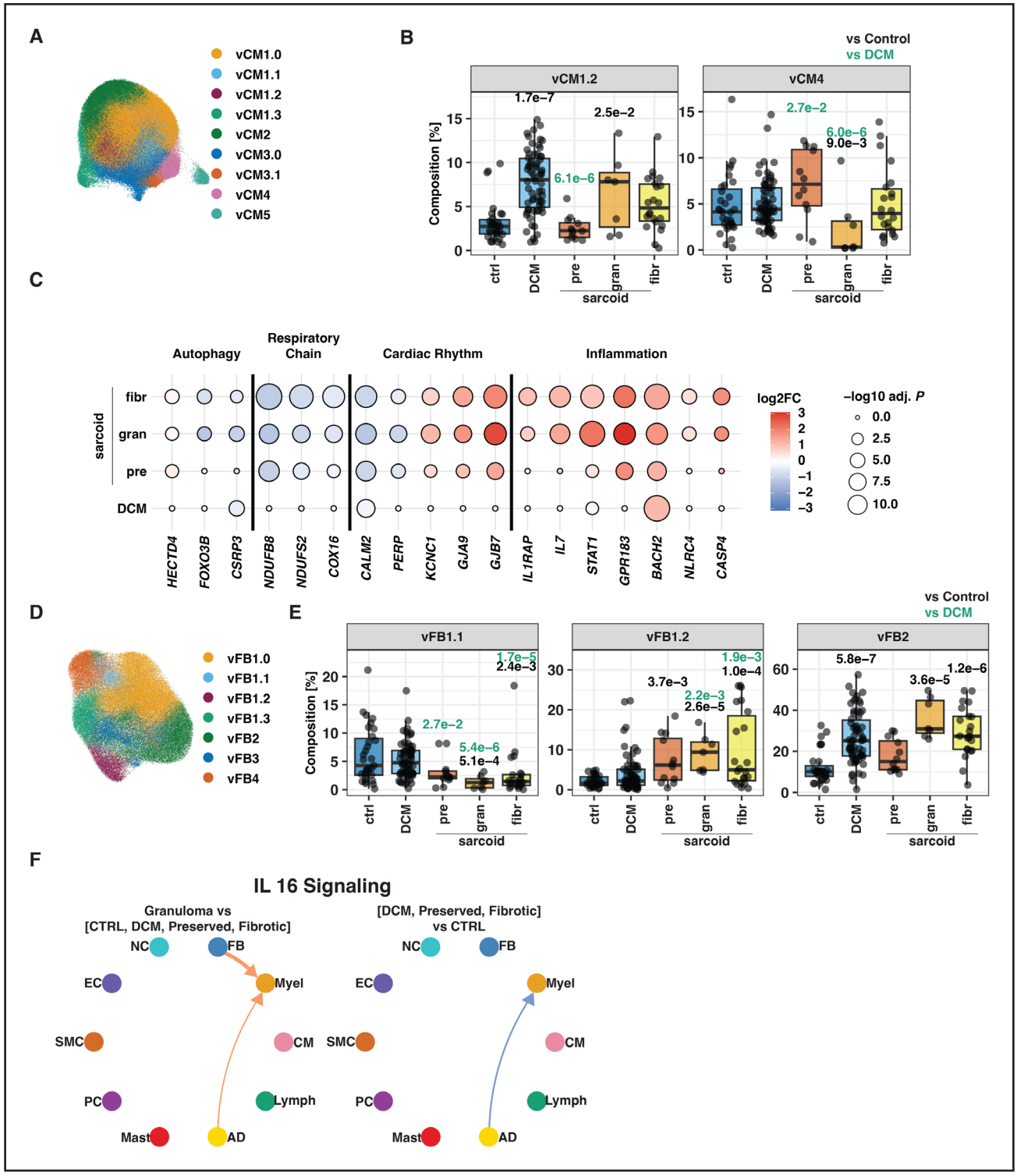

Figure 3. Transcriptional remodeling of cardiomyocytes and fibroblasts in cardiac sarcoidosis.
A, Uniform manifold approximation and projection distinguishing 9 cardiomyocyte transcriptional states (ventricular cardiomyocytes [vCMs]), denoted by colors, in control, dilated cardiomyopathy (DCM), and cardiac sarcoidosis (CS) tissues. **B**, Proportional abundance of vCMs 1.2 and 4.0 in preserved (pre), granulomatous (gran), and fibrotic (fibr) CS compared with DCM and control tissues. **C**, Relative cardiomyocyte expression of genes involved in autophagy, oxidative phosphorylation, cardiac conduction, rhythm regulation, and inflammation in CS and DCM tissues. Color represents log2FC relative to expression in control tissues; dot size reflects the −log10 Benjamini-Hochberg–adjusted *P* value. **D**, Uniform manifold approximation and projection of fibroblast transcriptional states (ventricular fibroblasts [vFBs]) denoted by colors in control, DCM, and CS tissues. **E**, Proportional abundance in vFB 1.1, 1.2, and 2.0 in preserved (pre), granulomatous (gran), and fibrotic (fibr) CS compared with DCM and control tissues. **F**, Graphic representation of increased IL-16 (interleukin-16) signaling from fibroblast to myeloid cells selectively in granulomatous CS sarcoid tissues. AD indicates adipocytes; CM, cardiomyocytes; EC, endothelial cells; FB, fibroblasts; Lymph, lymphoid cells; Myel, myeloid cells; NC, neuron cells; PC, pericytes; and SMC, smooth muscle cells.

protein expressed in skin, lung, and cardiac fibroblasts, and in cardiomyocytes, rare missense variants are associated with arrhythmogenic cardiomyopathies that typically arise from altered desmosome proteins.[20] Sarcoid cardiomyocytes upregulated the potassium channel *KCNC1*, involved in phase 1 repolarization,[21] and gap junction protein genes *GJA9* and *GJB7*, which regulate intercellular coupling.[22]

Dysregulated transcripts in neuronal cells (Table S6), comprising ≈1% of cardiac cells (Figure 1D), may contribute to electrophysiologic instability in CS. Neuronal cells upregulated *GRIK2* (glutamate ionotropic receptor kainate type subunit 2), encoding a kainate-type glutamate receptor,[23] and *NRXN1* (neurexin-1), encoding a key synaptogenic protein,[24] potentially increasing neurocardiac excitability.

Inflammatory transcriptional signatures were pronounced in cardiomyocytes from granulomatous and fibrotic regions. Cardiomyocytes upregulated *IL1RAP* and its effector, *STAT1*, inferring activated IL-1 (interleukin-1) pathways.[25] Upregulation of *GPR183* and *IL7*—genes associated with lymphocyte migration, development, and survival[26,27]—indicated that cardiomyocytes directly contributed to inflammation. Increased expression of the necroptosis repressor *BACH2*[28] and of *NLRC4*, *NAIP*, and *CASP4*, *CASP5*, and *CASP8*—central mediators of the inflammasome and pyroptosis[29]—implied that cardiomyocytes activated pyroptotic cell death pathways. If confirmed, this observation could inform therapeutic interventions, such as the Food and Drug Administration–approved antipyroptosis drug disulfiram[30] in CS.

Taken together, these data demonstrated that cardiomyocytes in CS are progressively compromised by dysregulated energetic and electromechanical genes and concurrently activate inflammatory gene programs.

Fibroblasts Remodel ECM and Drive Proinflammatory Signaling

Abundance of fibroblast states (ventricular fibroblasts [vFBs])[31] indicated expansion of profibrotic vFB2, demarcated by *POSTN* and *FAP*,[32] in fibrotic and granulomatous CS and in DCM (Figure 3E, Figure S9, and Table S3). Unlike DCM, CS also upregulated antifibrotic vFB1.2, characterized by *SMAD6*[33] expression with accompanying loss of vFB1.1. These patterns suggested distinct fibroblast-mediated ECM remodeling in CS and DCM. Despite reduced abundances in CS, vFB1.1 increased *CCL19* expression >200-fold versus control (P=8.6e-10; Table S6). *CCL19*-producing fibroblasts promote tertiary lymphoid structures (TLS) in cancers, enhancing local immunoglobulin production by B cells[34] and contributing to autoimmune thyroiditis.[35]

Fibroblasts (and adipocytes) in granulomatous CS selectively upregulated the chemoattractant *IL16*[36] (Figure 3F). Lack of augmented IL-16 (interleukin-16) signaling in preserved and fibrotic CS and DCM may indicate a granuloma-specific fibroblast program for immune cell recruitment. As such, the cells, similar to cardiomyocytes, were affected by and participated in sustaining local inflammatory processes in CS.

Myeloid States Highly Enriched in CS

Seven of 9 myeloid states in CS mirrored those previously identified in DCM.[8] In addition, CS was enriched for 2 macrophage states: MP_GPNMB and MP_GPNMB_CHI3L1 (Figure 4A). MP_GPNMB, modestly increased in DCM and scarce in preserved CS, was significantly elevated (≈6%) in granulomatous regions (Figure 4B and Figure S10). MP_GPNMB expressed M2 transcriptional signatures (Figure 4C), including *PPARG* and *DHRS9*, and *GPNMB*, a marker for reparative macrophages in the heart.[37] These cells also upregulated *CYP27A1*, an IFN-γ (interferon-γ)–induced, vitamin D3–activating enzyme that enhances Toll-like receptor–mediated antimicrobial responses, which is inappropriately activated in granulomatous sarcoidosis.[38]

MP_GPNMB_CHI3L1, nearly absent in control and DCM tissue, comprised ≈25% of CS myeloid cells and was most abundant in granulomatous regions (Figure 4A and 4B). Like MP_GPNMB, MP_GPNMB_CHI3L1 expressed *GPNMB* and *CYP27A1*, highlighting transcriptional relatedness, but was enriched for *CHI3L1* (encoding gp39 [glycoprotein-39]), a mediator of proinflammatory cytokine effects,[39] and *TNFSF13B* (encoding BAFF [B-cell activating factor]), involved in B-cell production of autoimmune antibodies[40] (Figure 4C). MP_GPNMB_CHI3L1 cells also upregulated *CD38*, *STAT1*, and *SLAMF7*, inferring an IFN-γ–promoted proinflammatory phenotype.[41,42]

Notably, MP_GPNMB_CHI3L1 expressed *DCSTAMP*, encoding a cell-fusion protein required for multinucleated giant osteoclasts.[43] Consistent with *DCSTAMP* expression, spatial transcriptomics demonstrated *CHI3L1* and *GPNMB* coexpression in morphologically defined multinucleated giant cells (Figure 4D; top panel), whereas cells expressing only *GPNMB* were mononuclear (Figure 4D; bottom panel). Based on these distinct morphologic and transcriptional profiles (Figure 4C), we denoted multinucleated giant cells in CS granulomas as MP_GPNMB_CHI3L1 cells.

Gene Ontology enrichments (Figure 4E) indicated that MP_GPNMB_CHI3L1 and MP_GPNMB shared expression profiles linked to foam cell differentiation and tissue remodeling, whereas only MP_GPNMB_CHI3L1 genes were enriched for pathways governing leukocyte recruitment and activation. Additional studies of key genes expressed in these macrophage states may expand understandings of their distinct functions in CS and inflammatory diseases.

These observations highlight the dynamic balance in CS between immune activation (MP_GPNMB_CHI3L1:

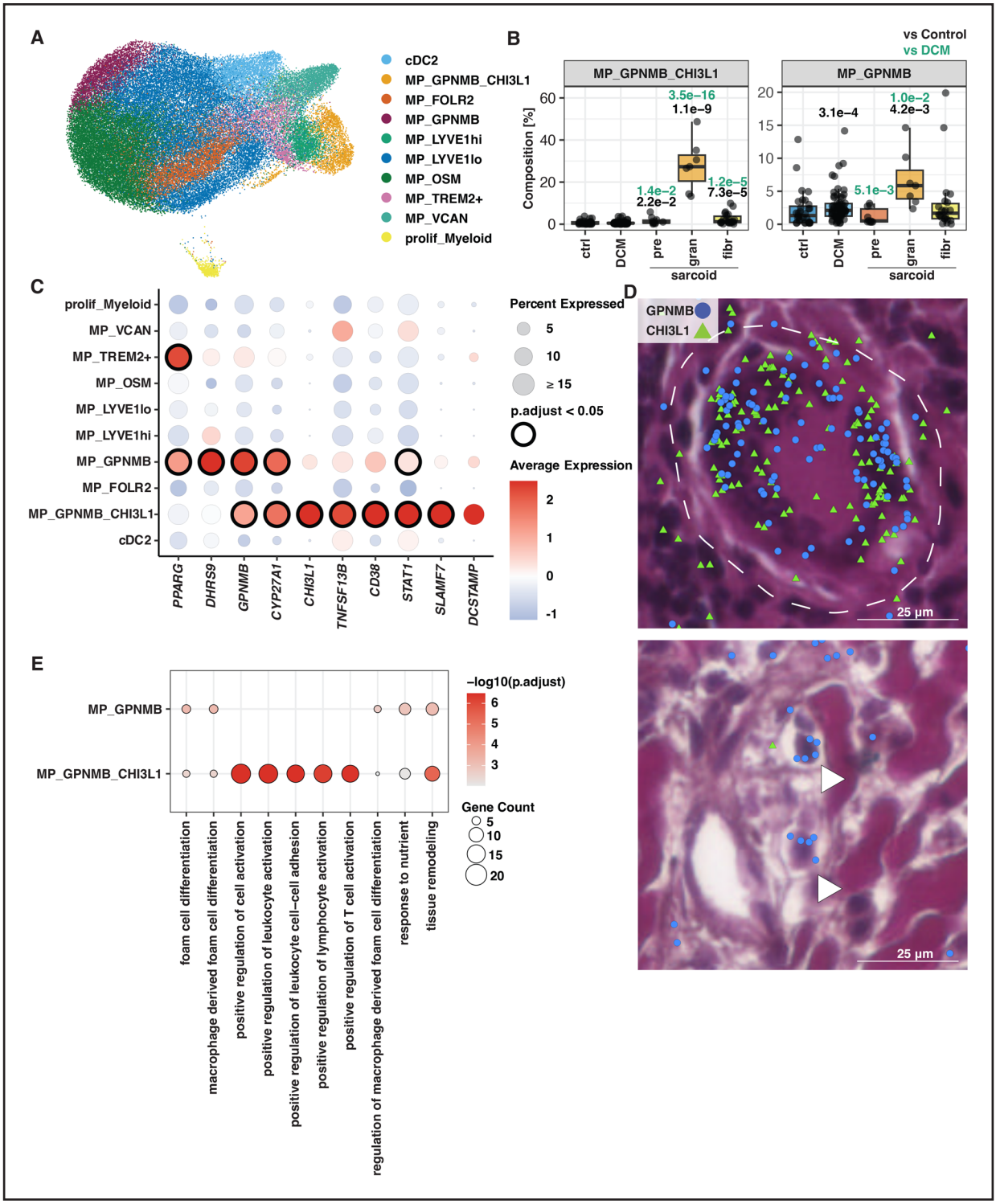

Figure 4. Two specialized myeloid states enriched in cardiac sarcoidosis.
A, Uniform manifold approximation and projection embedding of myeloid nuclei, colored by transcriptional states labeled with specific marker genes, from control, dilated cardiomyopathy (DCM), and cardiac sarcoidosis tissues. **B**, Box plots comparing abundances of myeloid states in different conditions. Benjamini-Hochberg–adjusted *P* values with false discovery rate ≤0.05 are displayed for differences versus controls (black) and DCM (green). **C**, Dot plot of scaled mean expression for top marker genes defining each state. **D**, Spatial transcriptomics and in situ hybridization of tissue validated macrophage state-specific expression of *CHI3L1* (green triangles) and *GPNMB* (blue dots), overlaid on hematoxylin & eosin–stained sections identifying a multinucleated giant cell (dashed white circle; top panel). The *GPNMB* signal is also present in mononuclear macrophages (white arrowheads; bottom panel). **E**, Gene Ontology enrichment for biologic-process terms associated with genes expressed by *GPNMB*-positive and *CHI3L1*-positive macrophages. Colors of dots denote −log10 adjusted *P* value; sizes denote numbers of expressed genes in each term. cDC2 indicates dendritic cells; MP, macrophages; and prolif, proliferating.

proinflammatory, fusion-competent state closely linked to multinucleated giant cells) and tissue repair (MP_GPNMB: M2-like signals). We nominate CHI3L1 (chitinase-3-like protein 1) and the MP_GPNMB_CHI3L1 states as plausible therapeutic targets for rebalancing immune processes in CS, for example by using the recently developed humanized anti-CHI3L1 antibody.[44]

Distinct Lymphocyte Subpopulations Reveal Distinct Immune Responses in Granulomatous and Fibrotic Regions of Sarcoidosis

Broader diversity of lymphocyte populations was revealed by TRUST4[11] analyses, which identified an additional 4993 nuclei expressing rearranged V(D)J genes that were initially excluded by quality control filtering, including highly differentiated immunoglobulin-producing B cells (Supplemental Methods). These were integrated with the lymphoid nuclei from the main snRNA-seq pipeline (Supplemental Methods). More B-cell receptor than T-cell receptor sequences were identified by the TRUST4 algorithm.

Lymphocyte populations were categorized as T cells plus natural killer cells or B cells (Figure 5A–5C). Within the T and natural killer cell compartment, we identified 7 states (Figure 5A and 5D), 2 expressing *RORC*, the master transcription factor driving Th17 differentiation.[45] CD4_T_RORC_RBPJ cells concurrently expressed *RBPJ*, indicating a pathogenic Th17 phenotype.[46] Other notable transcripts included *STAT1*, associated with IFN-γ–driven Th1 polarization,[47] and *DAPK2*, upregulated in activated T cells, where it dampens mTORC1 (mammalian target of rapamycin complex 1) and suppresses T- and B-cell interactions.[48] CD4_T_BAFF cells expressed *RORC* along with *TNFSF13B* (BAFF) and the T-cell receptor activation marker *RASGRF2*,[49] implying roles in B-cell activation and autoimmunity.[40] Both RORC-expressing cell states shared transcripts including *CHD7*, involved in T-cell development,[50] and *DPP4*, an activated lymphocyte marker.[51]

Six distinct B-cell states were delineated (Figure 5C and 5D). Transitional B cells expressed developmental genes, *EBF1*, *PAX5*, and the BAFF receptor *TNFRSF13B*, associated with humoral autoimmunity.[52,53] *IGHD* and *IGHM* coexpression defined naïve B cells,[54] whereas *BCL6* expression marked a germinal center-like state.[55] *ITGAX* expression characterized an age-associated B-cell state linked to humoral autoimmunity.[56] Plasma cells were identified based on *PRDM1* expression.[57] B cells with low transcriptional counts were inferred to have a quiescent memory state. The considerable B-cell diversity suggested a complex progression of B-cell activation and differentiation in CS tissues.

Immune cell abundances in CS varied among histopathologic regions (Figure 5F). CD4_T_RORC_RBPJ cells were most abundant in granulomatous CS compared with control samples (15.8%±1.9% versus 3.7%±0.8%; *P*=2.9e-4), with modest increases in fibrotic CS, like DCM. CD4_T_reg cells likewise showed greatest abundance in granulomatous CS. Fibrotic CS were enriched for transitional B cells (5.5%±1.4%) compared with DCM (2%±0.3%; *P*=1.6e-4) and control tissues (4.1%±1%; *P*=5.3e-3), as were plasma cells (2.3%±0.3% versus DCM 1.7%±0.3%; *P*=3.8e-4; versus control 2.2%±0.3%; *P*=3.6e-3). These data implied that pathogenic Th17 cells were active in granuloma formation, with concurrent enrichment of regulatory T cells, plausibly moderating this process, whereas fibrotic regions had abundant B cells with transitional B cells and plasma cell differentiation.

V(D)J sequences of B- and T-cell clones were identified in CS, with CDR3 (complementarity-determining region 3) sequences defining clonotypes (Figure 5G and Supplemental Methods). Comparisons with germline sequences revealed variants arising during V(D)J rearrangement in primary lymphoid organs, and additional variants within tissue-resident B cells, indicative of somatic hypermutation during clonal expansion. Cardiac B cells showed more variants than T cells (5.93±2.2 variants/100 bp versus 0.77±0.33 variants/100 bp).

B-cell and T-cell clone sizes (defined as numbers of cells comprising each clone) varied by disease status. Control, DCM, and preserved CS tissues had few, small B-cell clones (maximum cells per clone=6; Figure 5H, left panel). Both granulomatous and fibrotic CS tissues had more and larger clones, including 1 clone with 89 B cells (*P*=8e-4 compared with controls) and comprised up to 14.9% of B cells with rearranged antibody genes in the CS tissue (sample SS-1065_SP; Table S8). T-cell clone sizes did not differ among control, sarcoid, or DCM samples, and were considerably smaller than B-cell clones (Figure 5H, right panel).

Using CS hearts with multiple tissue samples from different cardiac regions (Figure 1A), we identified identical B- and T-cell clonotypes across spatially separated sites. In participant A0069, 1 B-cell clone spanned the LVFW and IVS, and in participant A0239, 1 T-cell clone resided in separated LVFW segments. Similarly, 3 B-cell and 2 T-cell clones were found in both the right ventricular free wall and IVS from participant SS-1065 (data not shown).

Collectively, the increased B-cell abundances with transcriptional signatures of intracardiac B-cell maturation indicated vigorous B-cell clonal expansion with somatic hypermutation and intracardiac dissemination. Combined with enrichment of T-cell states, these findings implied activation of coordinated adaptive immunity that promoted granuloma formation and fibrotic remodeling in CS.

Spatially Defined Immune Microenvironments Characterize TLS Formation in CS

We assessed whether distinct immune cell types formed unique spatial clusters within CS tissues by refining

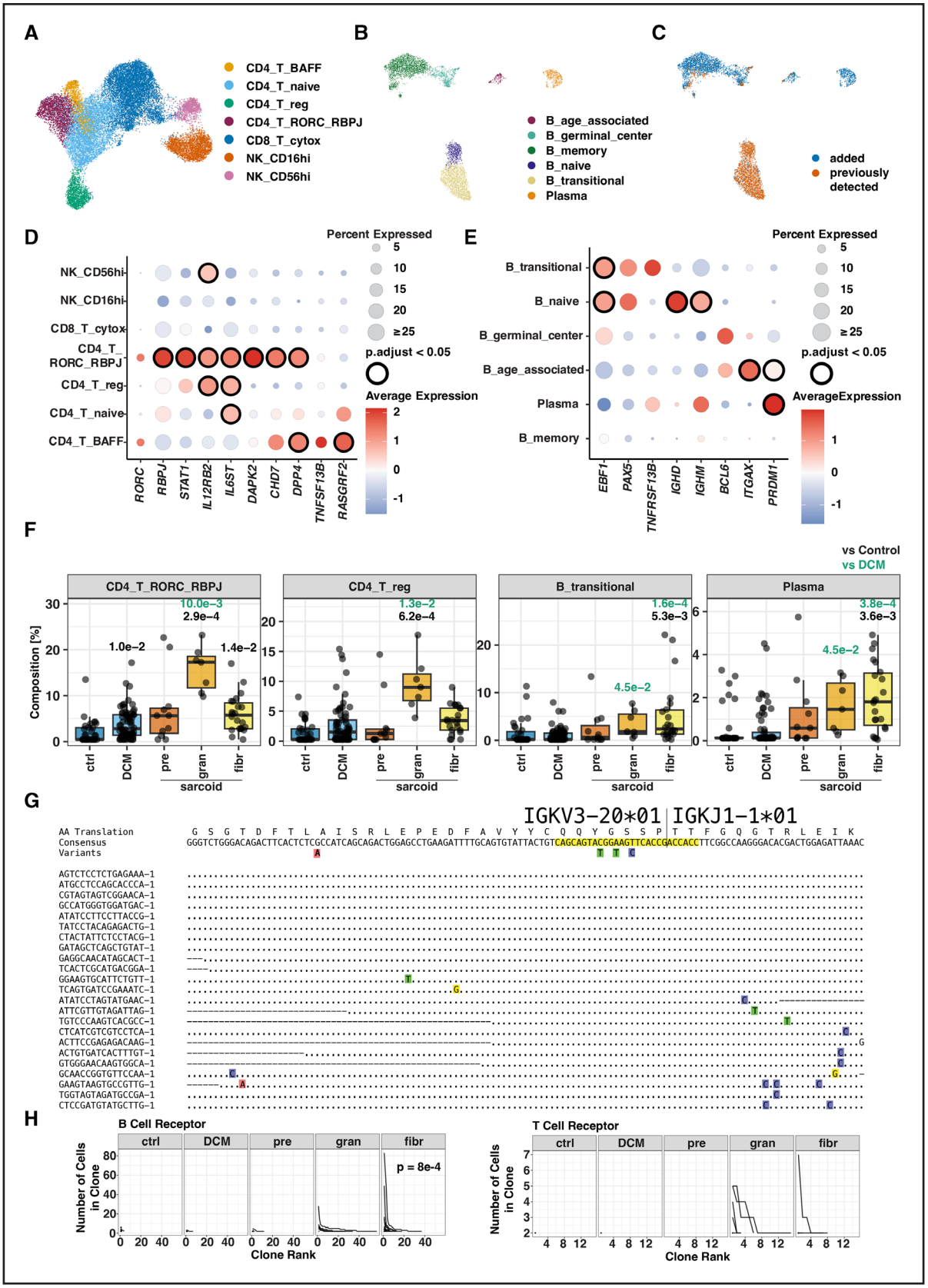

Figure 5. Pathogenic T cells and clonally expanded, activated B cells in cardiac sarcoidosis.
A, Uniform manifold approximation and projection embedding of T cell and natural killer (NK) cell nuclei, colored by transcriptional states labeled with specific marker genes, from control, dilated cardiomyopathy (DCM), and cardiac sarcoidosis tissues. **B** and **C**, Uniform manifold approximation and projection of B-cell nuclei, colored by B-cell states (**B**) and by nuclei identified by standard pipeline (brown) or added after (*Continued*)

Figure 5 Continued. TRUST4 analyses of rearranged V(D)J transcripts (**C**). **D** and **E**, Dot plots of scaled marker-gene expression for (**D**) T and NK cell states defined in panel **A** and (**E**) B-cell states defined in panel **B**. **F**, Box plots comparing the proportions of lymphoid states across conditions; Benjamini-Hochberg–adjusted *P* values for differences in cardiac sarcoidosis versus controls (black) and DCM (green) with false discovery rate ≤0.05. **G**, Representative alignment of immunoglobulin variable (V) and joining (J) region sequences from a single B-cell clone. A "parental" light chain sequence (including CDR3 [complementary-determining region 3] sequences, yellow) is shown, highlighting nucleotides (colored boxes) that differ from germline (IGKV3-20) sequences. Below are sequences from unique cells (identified by barcodes) carrying the parental clonotype (▪) and additional variants (highlighted nucleotides), indicative of somatic hypermutation. **H**, Rank-abundance curves illustrating clone-size distributions (cells per clone) for each sample, ordered by total clone count and grouped by diagnosis. *P* values are shown for groups with significant enrichment of expanded clones containing ≥6 cells for B-cell receptor or ≥2 cells for T-cell receptor—the largest clone sizes observed in control samples.

neighborhood analyses and incorporating MP_GPNMB_CHI3L1 cells (comprising multinucleated giant cells) and mononuclear myeloid, B, and T cells with the initial cell-type annotations (Figure 2D–2G). Within granulomatous and fibrotic regions, immune neighborhoods clustered into 3 distinct niches (Figure 6A). T-cell neighborhoods had 24% T cells, few (7%) B cells, and 18% myeloid cells. Myeloid neighborhoods had the greatest MP_GPNMB_CHI3L1 abundance (39%) and 21% to 22% myeloid and T cells. B-cell neighborhoods had almost 50% B cells, 24% T cells, 11% MP_GPNMB_CHI3L1, and 6% mononuclear myeloid cells.

Within granulomatous CS, B-cell neighborhoods were rare (0.1%), but comprised 1.4% of neighborhoods in fibrotic CS (Figure S18). Notably B-cell neighborhoods in fibrotic CS were clustered into TLS (Figure 6D), characteristic of chronically inflamed tissues, and previously identified in allograft transplanted heart tissues.[58] Fibrotic CS tissues also were enriched in plasma cells (Figure 5F), further supporting that clustered cells formed TLS. Similar to previous snRNA-seq studies that reported poor detection of prototypical immune cell surface markers,[59] we identified few transcripts encoding CD20 and CD23—proteins that demarcate B cells and follicular dendritic cells within TLS.[60] We therefore used immunofluorescence staining and observed aggregates of CD20-positive B cells and CD23-positive follicular dendritic cells forming regional clusters, consistent with TLS structures in fibrotic CS tissues (Figure 6E and Supplemental Methods). Similar cellular aggregates were not observed in control or DCM sections (Figure S12). These data suggested that spatially defined B-cell neighborhoods constitute TLS, and the myeloid-cell neighborhoods reflect core granuloma cells with enrichment of MP_GPNMB_CHI3L1.

TLS foster the production of autoreactive B cells targeting autoantigens by enabling B-cell maturation and clonal expansion outside of secondary lymphoid tissues.[61] Notably, *CCL19*, which promotes TLS formation, was most highly expressed in myeloid neighborhoods; its cognate receptor, *CCR7*, was highest in B-cell neighborhoods (Figure 6F), implying the cellular targets of *CCL19* signaling are preferentially located in B-cell neighborhoods. Moreover, *CCR7* expression significantly correlated with the maximum size of B-cell clones (R=0.602, $P=1.43\times10^{-9}$; Figure 6G), further supporting a role for *CCL19-CCR7* signaling activity in B-cell expansion within CS. These data support the conclusion that specialized immune microenvironments in CS promote neighborhoods that form TLS with the potential to produce autoreactive antibodies that could contribute to evolving histopathology during disease progression.

B-Cell Clones in CS Tissue Encode Autoreactive Antibodies Targeting Cardiac Proteins

snRNA-seq defined full-length heavy and light chain sequences of 16 different clones obtained from 5 different participants. We synthesized recombinant antibodies using the full-length V(D)J sequences encoding both immunoglobulin heavy and light chains from clonally expanded B cells within fibrotic or granulomatous tissues from 5 CS hearts (Table S7). Recombinant antibodies were screened by phage immunoprecipitation sequencing to discover target epitopes using duplicated libraries containing ≈600 000 overlapping peptides spanning the human peptidome,[9] along with >120 000 microbial peptides derived from viral, bacterial, protozoan, fungal, and archaeal organisms, as well as plant- and animal-derived allergens.[10] Commercially available antibodies targeting B-tubulin, caspase, and plectin served as positive controls (Supplemental Methods).

Positive control monoclonal antibodies (plectin and caspase; Table S8) and a polyclonal antibody (B-tubulin; Table S8) bound their target peptides with high confidence (*z* scores >100) and also reacted with other human peptides. None of the 16 recombinant CS antibodies reacted with nonhuman peptides or allergens, and 5 had no reactivity to any human peptide. Eleven CS antibodies were highly immunoreactive to 34 different human proteins, including 10 antibodies that reacted to contiguous peptides with overlapping epitope sequences (Table S8).

The targets of these immunoreactive CS antibodies included proteins previously implicated in inflammation (eg, USP5 [ubiquitin-specific protease 5] in Kawasaki disease[62]) or identified as autoantigens, including Lambert–Eaton myasthenic syndrome (ERC1 [ELKS/Rab6-interacting/CAST family member 1][63]) and Takayasu arteritis (SPATA7 [spermatogenesis-associated 7][64]). Other immunoreactive proteins function in cytoskeleton

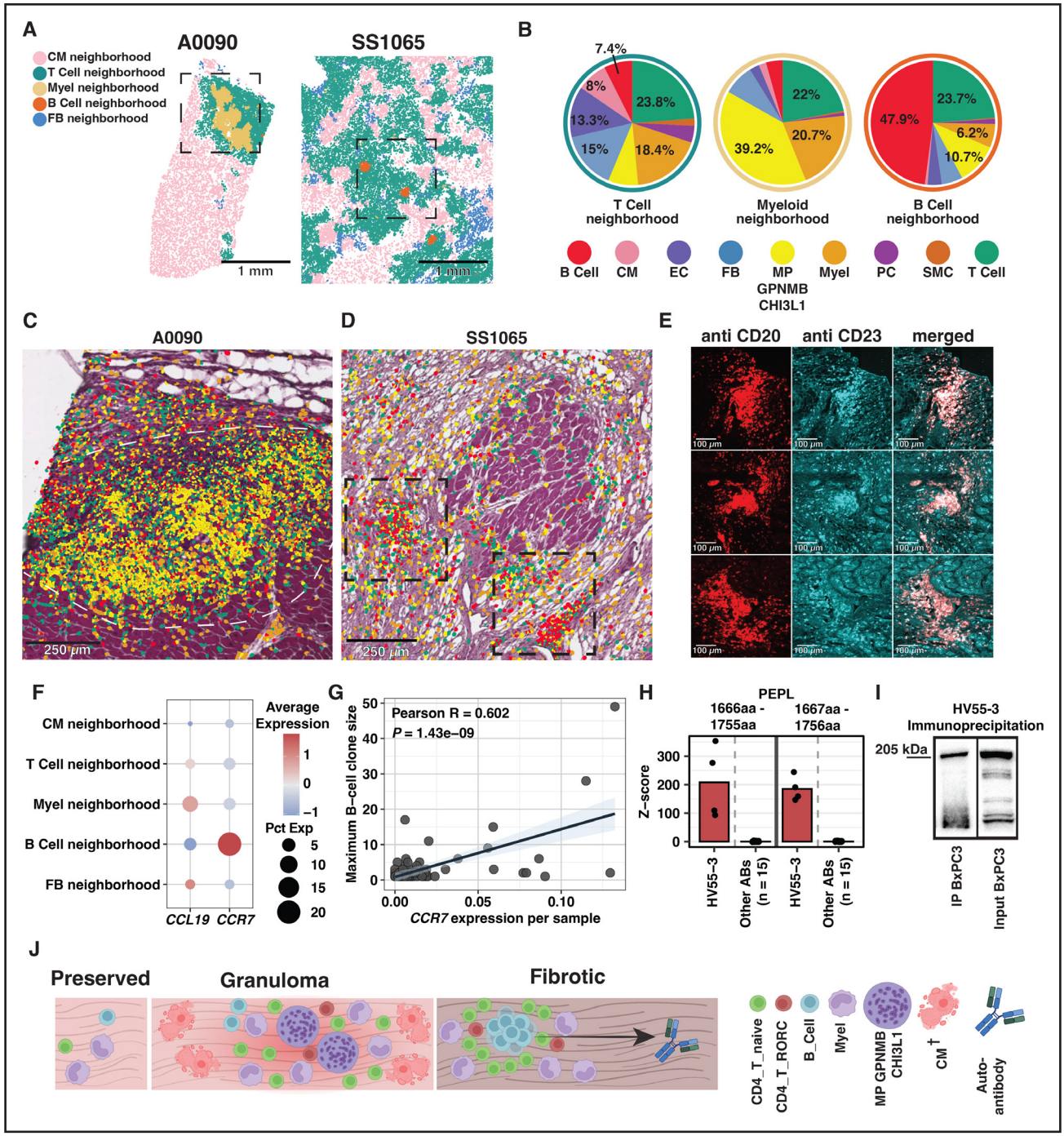

Figure 6. Tertiary lymphoid structures in fibrotic regions of cardiac sarcoidosis.
A, Representative spatial transcriptomics images from cardiac sarcoidosis hearts (A0090 and SS1065) identified cardiomyocyte (CM)–enriched and fibroblast (FB)–enriched neighborhoods (defined in Figure 2D–2G) and immune-enriched neighborhoods refined into B cell, T cell, and myeloid (Myel) neighborhoods. **B**, Circle plots depicting the cellular composition within expanded immune cell neighborhood. **C**, Hematoxylin & eosin–stained section of panel **A** (boxed) with a granuloma (white dashed lines) containing multinucleated giant cells overlaid with MP_GPNMB_CHI3L1 (yellow), mononuclear myeloid (orange), T-cell nuclei (green), and B-cell nuclei (red) identified by spatial transcriptomics. Note sparsity of immune cells in the preserved region below the granuloma. **D**, Hematoxylin & eosin–stained section of panel **A** (boxed) showing a fibrotic region surrounding preserved region, overlaid with nuclei (defined in **C**), identified by spatial transcriptomics. The fibrotic region contained tertiary lymphoid structures (TLS; boxed) with B, T, mononuclear myeloid, and MP_GPNMB_CHI3L1 cells. **E**, Immunofluorescence staining of cardiac sarcoidosis myocardial tissue depicting TLS, with CD20 highlighting clustered B cells and CD23 highlighting follicular dendritic cells. **F**, Dot plot showing scaled expression of *CCL19* and *CCR7* across spatial neighborhoods in cardiac sarcoidosis tissues. **G**, Scatterplot showing the correlation between *CCR7* expression and maximum B-cell clone size across all analyzed samples. **H**, Bar plot showing PhIP-seq *Z* scores for HV55-3 and all other recombinant antibodies against 2 overlapping Periplakin peptides. **I**, Immunoprecipitation of BxPC3 cell lysate using antibody HV55-3, shown alongside full lysate input. **J**, A model of cardiac sarcoidosis progression, in preserved, granulomatous, and fibrotic regions. EC indicates endothelial cells; PC, pericytes; and SMC, smooth muscle cells.

organization and specialized intercellular junctions, including SPECC1L (sperm antigen with calponin homology and coiled-coil domains 1-like), an adherens junction protein,[65] and PPL, an autoantigen in paraneoplastic pemphigus[66] and component of desmosomes[67] that support structural integrity in epithelial cells within skin, lung, and myocardium—tissues prominently involved in sarcoidosis.[1] Overall, CS antibodies were highly immunoreactive to 14 proteins that were previously identified as human autoantigens (Table S8).

We validated the activity of 1 representative antibody, HV55-3, which comprised 6% (29 cells) of all B cells in the A0090 LV sample and targeted 2 linear PPL peptides (Table S8). HV55-3 robustly immunoprecipitated native PPL from protein extracts of the PPL-expressing BxPC3 cell line[68] (Figure 6I).

We propose a working model that integrates the potential pathogenic signals identified by snRNA-seq, spatial transcriptomics, and PhIP-seq in CS myocardium (Figure 6J). This schematic outlines a potential sequence linking inflammatory cell infiltration, granuloma formation, cardiomyocyte injury, fibrotic remodeling, TLS organization, and B-cell–mediated autoimmunity. The proposed sequence, supported by multi-omic data, provides a framework for mechanistic studies and potential therapeutic targets in CS.

DISCUSSION

Through comprehensive analyses of CS tissues by snRNA-seq, spatial transcriptomics, V(D)J profiling, and PhIP-seq, we identified molecules and pathways that drive cardiac remodeling with unique histopathology in this enigmatic disorder. Differentially expressed genes in CS could compromise electrophysiology and energetics and incite inflammation to promote cardiomyocyte loss and fibroblast expansion, and propel HF. Some dysregulated genes and pathways were shared with DCM, but many were distinctive. Most notably, CS profoundly altered immune processes that promoted granuloma formation and autoimmune activation. By precise definition of these signals, we identified new potential CS therapeutic targets.

A pivotal design of these studies was initial assessment of histopathologic regions—preserved, granulomatous, and fibrotic—which were individually or multiply present in CS hearts. Each of these regions had distinctive properties in comparison with normal and DCM hearts. The cellular composition of preserved CS tissues resembled healthy myocardium but altered gene expression and immune cell polarization indicated early signals of active disease. Granulomatous regions displayed multinucleated giant cells, the canonical diagnostic pathology of CS, with intense immune activities activated by specific cells, cytokines, and transcriptional programs. Fibrotic regions, notable for marked cardiomyocyte depletion, abundant fibroblasts, and increased ECM, showed retention of robust immune infiltrates and, unexpectedly, formation of TLS. The consequence of these cellular processes, a burnt-out myocardium, also characterizes DCM, but the regional diversity with distinct immune cell properties indicated profoundly different mechanisms for adverse cardiac remodeling.

Spatial transcriptomics were key to understanding these processes. By defining discrete neighborhoods in each CS region, we observed distinct spatial architectures. Combined with detailed transcriptional data, immune-rich neighborhoods were further classified into niches composed of lymphocyte and stromal cells, myeloid and giant cells, and highly enriched B-cell TLS. These findings underscored roles played by specialized immune cells in progressive remodeling after granulomas are resolved, an observation that indicated the need for prolonged therapy in CS.

The pervasive dysregulation of electrophysiologic genes in cardiomyocytes suggested plausible links to increased arrhythmic risks in CS, even when cardiac architecture was preserved. Downregulation of transcripts encoding electrophysiologic proteins, similar to pathogenic loss-of-function variants, when combined with inflammation, could increase arrhythmogenicity. Moreover, the regionally segregated abnormalities may contribute to limited efficacy of focal antiarrhythmic interventions, such as ablation, in comparison with systemic therapies, as was recently proposed.[69] Exploring the electrophysiologic consequences of dysregulated genes in CS may clarify mechanisms and therapeutic targets.

Fibroblasts, which are key contributors to ECM expansions in many forms of heart disease, had unique roles in CS, and heighten both inflammatory and fibrotic responses. Increased IL-16 expression in fibroblasts echoed findings in rheumatoid arthritis, where this cytokine sustains chronic inflammation.[70] Fibroblast production of *CCL19* likely enhanced TLS formation in CS, as in other disorders.[34] Targeting these proinflammatory fibroblasts presents novel therapeutic opportunities for CS.

CS analyses delineated 2 states of *GPNMB*-positive macrophages, with plausible functional differences that refined previous characterization of these cells in granulomatous tissues.[71,72] *GPNMB*-positive mononuclear cells exhibited immunosuppressive transcripts. Conversely, *GPNMB*-positive cells that expressed *CHI3L1* were consistently associated with multinucleated cells, highly enriched in granulomatous CS, and marked by proinflammatory polarization with *BAFF* expression, a key cytokine for B-cell maturation. These data suggested that interplay between opposing myeloid states may regulate granuloma dynamics and potentially provide levers for therapeutic intervention.

T cells displayed considerable phenotypic diversity, including pathogenic Th17-like populations and a

BAFF-producing subset capable of driving B-cell activation.[40] In line with these multiple sources of *BAFF*, we identified robust B-cell infiltration, clonal expansion, and somatic hypermutation in both fibrotic and granulomatous regions, reinforced by the local formation of TLS in CS.

The application of TRUST4 analyses to snRNA-seq provided remarkable insights into B-cell responses in CS. We provide the first evidence for clonally expanded myocardial B cells that produced patient-specific antibodies in CS. By synthesizing antibodies encoded by clonally expanded B cells (comprising >10% of rearranged B cells in CS tissues), we identified strong autoreactivity to proteins previously identified as autoantigens in other diseases, including PPL. This desmosome protein is also targeted by autoantibodies in paraneoplastic pemphigus,[66] a most unlikely coincidence.

Circulating autoantibodies directed against myocardial antigens occur in myocarditis that progresses to DCM,[73] suggesting substantial clinical relevance. From analyses of 66 DCM tissues with genetic and nongenetic pathogeneses, we identified neither intramyocardial B-cell clones nor evidence for TLS organization. We therefore suggest that TLS with clonal expansion of B cells and intramyocardial autoantibody production are not generic features of advanced HF but characteristic of CS, and potentially other inflammatory cardiomyopathies.

Factors that initiate sarcoidosis and CS remain unknown, but our analyses support an autoimmune component in pathogenesis. Moreover, as reconstruction of full-length antibodies from snRNA-seq sequence data is challenging and incomplete recovery of both heavy and light chains prevents synthesis and analyses of all clonally expanded antibodies, these analyses likely underestimated the breadth of the antigenic repertoire in CS. Among 16 reconstructed antibodies, 5 lacked reactivity, possibly reflecting conformational epitopes, post-translational modifications, or sequences spanning tile boundaries in PhIP-seq libraries. By contrast, 11 antibodies targeted 35 patient-specific autoantigens. Delineating the full autoantigenic repertoire will necessitate additional high-resolution, unbiased approaches to discern endogenous or exogenous sources of epitope, and functional studies to illuminate their pathogenic roles in sarcoidosis.

The finding of autoantibodies in CS that target a component of desmosomes and adherens junction (Table S8) was unexpected. CS shares clinical manifestations with arrhythmogenic DCM that arises from loss-of-function variants in genes encoding desmosome proteins, or rare desmosome autoantibodies[74,75]; our findings provide plausible explanations for these similarities. B-cell activation during cardiomyocyte injury may heighten arrhythmic risks in CS, arrhythmogenic cardiomyopathies, and other inflammatory cardiomyopathies. B-cell activation in fibrotic regions, devoid of granulomas, may indicate persistent or augmented autoimmunity as disease progresses. This hypothesis is supported by case reports of improvement in patients with advanced refractory sarcoidosis treated with the B-cell–depleting anti-CD20 monoclonal antibody rituximab.[76] Our studies indicate additional agents, such as *CHI3L1*-targeting therapies[44] or the *BAFF* inhibitor belimumab,[77] that warrant immunomodulatory analyses in CS.

Integrating the snRNA-seq, spatial transcriptomic, and PhIP-seq data from CS tissues, we propose a model (Figure 6G) that links evolving cellular and molecular processes to drive disease progression. In this framework, an undefined initiating stimulus creates a permissive environment for myeloid cell infiltration into the myocardium, with monocytes differentiating into GPNMB$^+$CH13L1$^+$ macrophages that participate in granuloma formation and drive expansion of myeloid, T cells, and B cells. The resulting proinflammatory milieu injures cardiomyocytes, promoting electrical remodeling and cell loss that stimulates ECM expansion by activated fibroblasts. As inflammatory signals wane, granulomas resolve and fibrosis emerges with immunomodulatory fibroblasts and T cells that promote TLS formation, B-cell expansion, and immunoglobulin diversification, including production of autoantibodies against cardiac proteins. Together these processes sustain inflammation and progression to HF.

Additional studies and mechanistic analyses may further advance insights into CS pathogenesis. Analyses of earlier changes in the cellular composition and molecular signals may improve identification of initiating signals. Clinical data that fully capture cardiac function and immunosuppressive therapies are also needed to define whether cellular compositions and molecular signals influence disease trajectories. Analyses of circulating as well as resident immune cells in other involved tissues may clarify the broader impact of autoantigens, informing mechanisms underlying the remarkable tissue tropism of sarcoidosis and increasing understanding of the adaptive immune response in this and other enigmatic diseases.

CONCLUSION

Our findings emphasize that CS is a spatially organized disease comprising 3 distinct tissue environments, sustained by complex immune dynamics and parenchymal cell dysfunction. Local interactions appear essential for B-cell autoimmunity and chronic tissue damage that may underpin life-threatening arrhythmias and HF. By combining single-cell V(D)J profiling with PhIP-seq, we discovered PPL and other autoimmune targets in CS. Application of this strategy may uncover unrecognized self- or exogenous-derived antigens across other enigmatic immune-mediated diseases. Understanding these pathogenic mechanisms should enable development of precise therapeutics that mitigate inflammatory damage, reducing fibrotic remodeling and ultimately improving

outcomes in CS and other challenging autoimmune disorders.

ARTICLE INFORMATION

Received January 8, 2026; accepted April 21, 2026.

Affiliations

Department of Genetics (M.N., G.V., K.J.B., Y.C., J.M.G., O.G.L., A. Verma, A.J.W., B.A.M., D.M.D., S.R.D., D.R., H.W., S.J.E., J.G.S., C.E.S.) and Howard Hughes Medical Institute, Division of Genetics, Program in Virology (S.J.E.), Cardiovascular Imaging Program, Department of Medicine (S.D.), and Cardiovascular Imaging Program, Department of Radiology (S.D.), Brigham and Women's Hospital, Harvard Medical School, Boston, MA. Department of Cardiology, University Heart and Vascular Center Hamburg, University Medical Center Hamburg-Eppendorf, Hamburg, Germany (M.N.). German Centre for Cardiovascular Research (DZHK), Partner Site North, Hamburg, Germany (M.N.). Division of Cardiovascular Medicine, Massachusetts General Hospital, Boston (K.J.B.). Biomedical Research Institute (Y.C.), Department of Pathology (J.K.), and Cardiovascular Center, Division of Cardiology (J.-B.P.), Seoul National University Hospital, Republic of Korea. Departments of Surgery (R.T.G., M.M.P., D.E.B.) and Pathology (C.G.), Duke University, Durham, NC. Division of Cardiology, Department of Medicine and Mazankowski Alberta Heart Institute, Faculty of Medicine and Dentistry, University of Alberta, Edmonton, Canada (A. Viveiros, G.Y.O.). Divisions of Cardiovascular Medicine (Y.K., C.E.S.) and Genetics (Y.K.) and Department of Pathology (R.N.M.), Brigham and Women's Hospital, Boston, MA. Medizinische Klinik und Poliklinik I and Gene Center Munich, LMU Munich, Germany (D.R.). German Centre for Cardiovascular Research (DZHK), Partner Site Munich Heart Alliance, Germany (D.R.). Massachusetts Consortium on Pathogen Readiness, Boston (S.J.E.). Department of Internal Medicine, Seoul National University College of Medicine, Republic of Korea (J.-B.P.).

Acknowledgments

The authors thank the patients and their families for participation in the study; Athanasios Ploumakis, Antonella Arruda de Amaral, and the personnel of the Spatial Technologies Unit, Beth Israel Deaconess Medical Center, Harvard Medical School Initiative for RNA Medicine (RRID: SCR_024905) for performing the 10X Genomics Xenium assays; and MicRoN (Microscopy Resources on the North Quad) Core for technical assistance. Several plots were generated with BioRender.com.

Sources of Funding

Supported by the German Research Foundation (grant 505244757 to Dr Neyazi); the Ministry of Health & Welfare, Republic of Korea, Boston–Korea Innovative Research Project (grant RS-2024-00403047 to Drs Choi and Park); the Heart and Vascular Center at Brigham and Women's Hospital Khoury Innovation Award (Dr Divakaran); the University of Alberta Hospital Foundation, Canadian Institute of Health Research, and Heart Stroke Foundation (Dr Oudit); the British Heart Foundation Challenge Award to CureHeart (BBC/F/21/220106 to Drs J.G. Seidman and C.E. Seidman); the National Heart, Lung, and Blood Institute (grant 5R01HL080494 to Drs J.G. Seidman and C.E. Seidman); and a gift from an anonymous donor (to Drs J.G. Seidman and C.E. Seidman).

Disclosures

Dr C.E. Seidman serves on the Board of Directors for Merck and the Scientific Advisory Board for Tenaya. Neither entity had any involvement related to the content of this article. The other authors report no relationships, activities, or interests related to the content of this article.

Supplemental Material

Methods
Tables S1–S8
Figures S1–S18
Uncropped gels
References 78–87

REFERENCES

1. Grunewald J, Grutters JC, Arkema EV, Saketkoo LA, Moller DR, Müller-Quernheim J. Sarcoidosis. *Nat Rev Dis Primers*. 2019;5:1–22. doi: 10.1038/s41572-019-0096-x
2. Kirkil G, Lower EE, Baughman RP. Predictors of mortality in pulmonary sarcoidosis. *Chest*. 2018;153:105–113. doi: 10.1016/j.chest.2017.07.008
3. Swigris JJ, Olson AL, Huie TJ, Fernandez-Perez ER, Solomon J, Sprunger D, Brown KK. Sarcoidosis-related mortality in the United States from 1988 to 2007. *Am J Respir Crit Care Med*. 2011;183:1524–1530. doi: 10.1164/rccm.201010-1679OC
4. Ekström K, Lehtonen J, Nordenswan H-K, Mäyränpää MI, Räisänen-Sokolowski A, Kandolin R, Simonen P, Pietilä-Effati P, Alatalo A, Utriainen S, et al. Sudden death in cardiac sarcoidosis: an analysis of nationwide clinical and cause-of-death registries. *Eur Heart J*. 2019;40:3121–3128. doi: 10.1093/eurheartj/ehz428
5. Rivière E, Jourde W, Gensous N, Demant X, Ribeiro E, Duffau P, Mercié P, Viallard J-F, Lazaro E. Efficacy and safety of Infliximab in systemic sarcoidosis according to GenPhenReSa organ-involvement phenotype: a retrospective study of 55 patients. *Respir Res*. 2024;25:124. doi: 10.1186/s12931-024-02758-6
6. ElRefai M, Menexi C, Roberts PR. Device therapy in cardiac sarcoidosis: current review, challenges, and future prospects. *J Innov Card Rhythm Manag*. 2024;15:6088–6094. doi: 10.19102/icrm.2024.15115
7. Litviňuková M, Talavera-López C, Maatz H, Reichart D, Worth CL, Lindberg EL, Kanda M, Polanski K, Heinig M, Lee M, et al. Cells of the adult human heart. *Nature*. 2020;588:466–472. doi: 10.1038/s41586-020-2797-4
8. Reichart D, Lindberg EL, Maatz H, Miranda AMA, Viveiros A, Shvetsov N, Gärtner A, Nadelmann ER, Lee M, Kanemaru K, et al. Pathogenic variants damage cell composition and single cell transcription in cardiomyopathies. *Science*. 2022;377:eabo1984. doi: 10.1126/science.abo1984
9. Larman HB, Zhao Z, Laserson U, Li MZ, Ciccia A, Gakidis MAM, Church GM, Kesari S, LeProust EM, Solimini NL, et al. Autoantigen discovery with a synthetic human peptidome. *Nat Biotechnol*. 2011;29:535–541. doi: 10.1038/nbt.1856
10. Xu GJ, Kula T, Xu Q, Li MZ, Vernon SD, Ndung'u T, Ruxrungtham K, Sanchez J, Brander C, Chung RT, et al. Comprehensive serological profiling of human populations using a synthetic human virome. *Science*. 2015;348:aaa0698. doi: 10.1126/science.aaa0698
11. Song L, Cohen D, Ouyang Z, Cao Y, Hu X, Liu XS. TRUST4: immune repertoire reconstruction from bulk and single-cell RNA-seq data. *Nat Methods*. 2021;18:627–630. doi: 10.1038/s41592-021-01142-2
12. Hao Y, Stuart T, Kowalski MH, Choudhary S, Hoffman P, Hartman A, Srivastava A, Molla G, Madad S, Fernandez-Granda C, et al. Dictionary learning for integrative, multimodal and scalable single-cell analysis. *Nat Biotechnol*. 2024;42:293–304. doi: 10.1038/s41587-023-01767-y
13. Chen Y, Chen L, Lun ATL, Baldoni PL, Smyth GK. edgeR v4: powerful differential analysis of sequencing data with expanded functionality and improved support for small counts and larger datasets. Published 2024. Accessed June 26, 2025. http://biorxiv.org/lookup/doi/10.1101/2024.01.21.576131
14. Xu S, Hu E, Cai Y, Xie Z, Luo X, Zhan L, Tang W, Wang Q, Liu B, Wang R, et al. Using clusterProfiler to characterize multiomics data. *Nat Protoc*. 2024;19:3292–3320. doi: 10.1038/s41596-024-01020-z
15. Korsunsky I, Millard N, Fan J, Slowikowski K, Zhang F, Wei K, Baglaenko Y, Brenner M, Loh P, Raychaudhuri S. Fast, sensitive and accurate integration of single-cell data with Harmony. *Nat Methods*. 2019;16:1289–1296. doi: 10.1038/s41592-019-0619-0
16. Zheng N, Shabek N. Ubiquitin ligases: structure, function, and regulation. *Annu Rev Biochem*. 2017;86:129–157. doi: 10.1146/annurev-biochem-060815-014922
17. Protasoni M, Zeviani M. Mitochondrial structure and bioenergetics in normal and disease conditions. *Int J Mol Sci* . 2021;22:586. doi: 10.3390/ijms22020586
18. Walsh R, Offerhaus JA, Tadros R, Bezzina CR. Minor hypertrophic cardiomyopathy genes, major insights into the genetics of cardiomyopathies. *Nat Rev Cardiol*. 2022;19:151–167. doi: 10.1038/s41569-021-00608-2
19. Crotti L, Spazzolini C, Tester DJ, Ghidoni A, Baruteau A-E, Beckmann B-M, Behr ER, Bennett JS, Bezzina CR, Bhuiyan ZA, et al. Calmodulin mutations and life-threatening cardiac arrhythmias: insights from the International Calmodulinopathy Registry. *Eur Heart J*. 2019;40:2964–2975. doi: 10.1093/eurheartj/ehz311
20. Gandjbakhch E, Vite A, Gary F, Fressart V, Donal E, Simon F, Hidden-Lucet F, Komajda M, Charron P, Villard E. Screening of genes encoding junctional candidates in arrhythmogenic right ventricular cardiomyopathy/dysplasia. *Europace*. 2013;15:1522–1525. doi: 10.1093/europace/eut224
21. Grant AO. Cardiac ion channels. *Circ Arrhythm Electrophysiol*. 2009;2:185–194. doi: 10.1161/CIRCEP.108.789081
22. Jongsma HJ, Wilders R. Gap junctions in cardiovascular disease. *Circ Res*. 2000;86:1193–1197. doi: 10.1161/01.res.86.12.1193
23. Nomura T, Taniguchi S, Wang Y-Z, Yeh N-H, Wilen AP, Castillon CCM, Foote KM, Xu J, Armstrong JN, Savas JN, et al. A pathogenic missense mutation in kainate receptors elevates dendritic excitability and synaptic integration

through dysregulation of SK channels. *J Neurosci*. 2023;43:7913–7928. doi: 10.1523/JNEUROSCI.1259-23.2023
24. Südhof TC. Synaptic neurexin complexes: a molecular code for the logic of neural circuits. *Cell*. 2017;171:745–769. doi: 10.1016/j.cell.2017.10.024
25. Ivashkiv LB. IFNγ: signalling, epigenetics and roles in immunity, metabolism, disease and cancer immunotherapy. *Nat Rev Immunol*. 2018;18:545–558. doi: 10.1038/s41577-018-0029-z
26. Winer H, Rodrigues GOL, Hixon JA, Aiello FB, Hsu TC, Wachter BT, Li W, Durum SK. IL-7: comprehensive review. *Cytokine*. 2022;160:156049. doi: 10.1016/j.cyto.2022.156049
27. Dickinson K, Yee EJ, Vigil I, Schulick RD, Zhu Y. GPCRs: emerging targets for novel T cell immune checkpoint therapy. *Cancer Immunol Immunother*. 2024;73:253. doi: 10.1007/s00262-024-03801-7
28. Gao P, Cao M, Jiang X, Wang X, Zhang G, Tang X, Yang C, Komuro I, Ge J, Li L, et al. Cannabinoid receptor 2-centric molecular feedback loop drives necroptosis in diabetic heart injuries. *Circulation*. 2023;147:158–174. doi: 10.1161/CIRCULATIONAHA.122.059304
29. Fu J, Schroder K, Wu H. Mechanistic insights from inflammasome structures. *Nat Rev Immunol*. 2024;24:518–535. doi: 10.1038/s41577-024-00995-w
30. Hu JJ, Liu X, Xia S, Zhang Z, Zhang Y, Zhao J, Ruan J, Luo X, Lou X, Bai Y, et al. FDA-approved disulfiram inhibits pyroptosis by blocking gasdermin D pore formation. *Nat Immunol*. 2020;21:736–745. doi: 10.1038/s41590-020-0669-6
31. Adami E, Kim Y, Zheng SL, Shvetsov N, Losert C, Maatz H, Barish S, Venturini G, López Anguita N, Shi Q, et al. Molecular landscape of hypertrophic cardiomyopathy across disease stages and genotypes. *Sci Transl Med*. (in press 2026).
32. Amrute JM, Luo X, Penna V, Yang S, Yamawaki T, Hayat S, Bredemeyer A, Jung I-H, Kadyrov FF, Heo GS, et al. Targeting immune–fibroblast cell communication in heart failure. *Nature*. 2024;635:423–433. doi: 10.1038/s41586-024-08008-5
33. Wrana JL, Attisano L. The Smad pathway. *Cytokine Growth Factor Rev*. 2000;11:5–13. doi: 10.1016/s1359-6101(99)00024-6
34. Zhang Y, Liu G, Zeng Q, Wu W, Lei K, Zhang C, Tang M, Zhang Y, Xiang X, Tan L, et al. CCL19-producing fibroblasts promote tertiary lymphoid structure formation enhancing anti-tumor IgG response in colorectal cancer liver metastasis. *Cancer Cell*. 2024;42:1370–1385.e9. doi: 10.1016/j.ccell.2024.07.006
35. Zhang Q-Y, Ye X-P, Zhou Z, Zhu C-F, Li R, Fang Y, Zhang R-J, Li L, Liu W, Wang Z, et al. Lymphocyte infiltration and thyrocyte destruction are driven by stromal and immune cell components in Hashimoto's thyroiditis. *Nat Commun*. 2022;13:775. doi: 10.1038/s41467-022-28120-2
36. Franz JK, Kolb SA, Hummel KM, Lahrtz F, Neidhart M, Aicher WK, Pap T, Gay RE, Fontana A, Gay S. Interleukin-16, produced by synovial fibroblasts, mediates chemoattraction for CD4+ T lymphocytes in rheumatoid arthritis. *Eur J Immunol*. 1998;28:2661–2671. doi: 10.1002/(SICI)1521-4141(199809)28:09<2661::AID-IMMU2661>3.0.CO;2-N
37. Ramadoss S, Qin J, Tao B, Thomas NE, Cao E, Wu R, Sandoval DR, Piermatteo A, Grunddal KV, Ma F, et al. Bone-marrow macrophage-derived GPNMB protein binds to orphan receptor GPR39 and plays a critical role in cardiac repair. *Nat Cardiovasc Res*. 2024;3:1356–1373. doi: 10.1038/s44161-024-00555-4
38. Liu PT, Stenger S, Li H, Wenzel L, Tan BH, Krutzik SR, Ochoa MT, Schauber J, Wu K, Meinken C, et al. Toll-like receptor triggering of a vitamin D-mediated human antimicrobial response. *Science*. 2006;311:1770–1773. doi: 10.1126/science.1123933
39. Yu JE, Yeo IJ, Han S-B, Yun J, Kim B, Yong YJ, Lim Y, Kim TH, Son DJ, Hong JT. Significance of chitinase-3-like protein 1 in the pathogenesis of inflammatory diseases and cancer. *Exp Mol Med*. 2024;56:1–18. doi: 10.1038/s12276-023-01131-9
40. Steri M, Orrù V, Idda ML, Pitzalis M, Pala M, Zara I, Sidore C, Faà V, Floris M, Deiana M, et al. Overexpression of the cytokine BAFF and autoimmunity risk. *N Engl J Med*. 2017;376:1615–1626. doi: 10.1056/NEJMoa1610528
41. Li W, Li Y, Jin X, Liao Q, Chen Z, Peng H, Zhou Y. CD38: A significant regulator of macrophage function. *Front Oncol*. 2022;12:775649. doi: 10.3389/fonc.2022.775649.
42. Simmons DP, Nguyen HN, Gomez-Rivas E, Jeong Y, Jonsson AH, Chen AF, Lange JK, Dyer GS, Blazar P, Earp BE, et al; Accelerating Medicines Partnership (AMP) RA/SLE Network. SLAMF7 engagement superactivates macrophages in acute and chronic inflammation. *Sci Immunol*. 2022;7:eabf2846. doi: 10.1126/sciimmunol.abf2846
43. Yagi M, Miyamoto T, Sawatani Y, Iwamoto K, Hosogane N, Fujita N, Morita K, Ninomiya K, Suzuki T, Miyamoto K, et al. DC-STAMP is essential for cell–cell fusion in osteoclasts and foreign body giant cells. *J Exp Med*. 2005;202:345–351. doi: 10.1084/jem.20050645
44. Yu H, Wang Z, Zhu B, Jia Z, Luo J, Han X, Chen H, Shao R. A humanized Anti-YKL-40 antibody inhibits tumor development. *Biochem Pharmacol*. 2024;225:116335. doi: 10.1016/j.bcp.2024.116335
45. Ivanov II, McKenzie BS, Zhou L, Tadokoro CE, Lepelley A, Lafaille JJ, Cua DJ, Littman DR. The orphan nuclear receptor RORgammat directs the differentiation program of proinflammatory IL-17+ T helper cells. *Cell*. 2006;126:1121–1133. doi: 10.1016/j.cell.2006.07.035
46. Meyer zu Horste G, Wu C, Wang C, Cong L, Pawlak M, Lee Y, Elyaman W, Xiao S, Regev A, Kuchroo VK. RBPJ controls development of pathogenic Th17 cells by regulating IL-23 receptor expression. *Cell Rep*. 2016;16:392–404. doi: 10.1016/j.celrep.2016.05.088
47. Hu X, Ivashkiv LB. Cross-regulation of signaling pathways by interferon-γ: implications for immune responses and autoimmune diseases. *Immunity*. 2009;31:539–550. doi: 10.1016/j.immuni.2009.09.002
48. Ni X, Wang Y, Wang P, Chu C, Xu H, Hu J, Sun J, Qi H. Death associated protein kinase 2 suppresses T-B interactions and GC formation. *Mol Immunol*. 2020;128:249–257. doi: 10.1016/j.molimm.2020.10.018
49. Ruiz S, Santos E, Bustelo XR. RasGRF2, a guanosine nucleotide exchange factor for Ras GTPases, participates in T-cell signaling responses. *Mol Cell Biol*. 2007;27:8127–8142. doi: 10.1128/MCB.00912-07
50. Gennery AR, Slatter MA, Rice J, Hoefsloot LH, Barge D, McLean-Tooke A, Montgomery T, Goodship JA, Burt AD, Flood TJ, et al. Mutations in CHD7 in patients with CHARGE syndrome cause T–B + natural killer cell + severe combined immune deficiency and may cause Omenn-like syndrome. *Clin Exp Immunol*. 2008;153:75–80. doi: 10.1111/j.1365-2249.2008.03681.x
51. Casrouge A, Sauer AV, Barreira da Silva R, Tejera-Alhambra M, Sánchez-Ramón S, Cancrini C, Ingersoll MA, Aiuti A, Albert ML. Lymphocytes are a major source of circulating soluble dipeptidyl peptidase 4. *Clin Exp Immunol*. 2018;194:166–179. doi: 10.1111/cei.13163
52. Jacobs HM, Thouvenel CD, Leach S, Arkatkar T, Metzler G, Scharping NE, Kolhatkar NS, Rawlings DJ, Jackson SW. BAFF promotes autoantibody production via TACI-dependent activation of transitional B cells. *J Immunol*. 2016;196:3525–3531. doi: 10.4049/jimmunol.1600017
53. Bullerwell CE, Robichaud PP, Deprez PML, Joy AP, Wajnberg G, D'Souza D, Chacko S, Fournier S, Crapoulet N, Barnett DA, et al. EBF1 drives hallmark B cell gene expression by enabling the interaction of PAX5 with the MLL H3K4 methyltransferase complex. *Sci Rep*. 2021;11:1537. doi: 10.1038/s41598-021-81000-5
54. Meffre E, Casellas R, Nussenzweig MC. Antibody regulation of B cell development. *Nat Immunol*. 2000;1:379–385. doi: 10.1038/80816
55. Basso K, Dalla-Favera R. BCL6: master regulator of the germinal center reaction and key oncogene in B cell lymphomagenesis. In: *Advances in Immunology*. Elsevier; 2010:193–210. https://linkinghub.elsevier.com/retrieve/pii/S0065277610050078
56. Cancro MP. Age-associated B cells. *Annu Rev Immunol*. 2020;38:315–340. doi: 10.1146/annurev-immunol-092419-031130
57. Tellier J, Shi W, Minnich M, Liao Y, Crawford S, Smyth GK, Kallies A, Busslinger M, Nutt SL. Blimp-1 controls plasma cell function through regulation of immunoglobulin secretion and the unfolded protein response. *Nat Immunol*. 2016;17:323–330. doi: 10.1038/ni.3348
58. Pipi E, Nayar S, Gardner DH, Colafrancesco S, Smith C, Barone F. Tertiary lymphoid structures: autoimmunity goes local. *Front Immunol*. 2018;9:1952. doi: 10.3389/fimmu.2018.01952.
59. Stoeckius M, Hafemeister C, Stephenson W, Houck-Loomis B, Chattopadhyay PK, Swerdlow H, Satija R, Smibert P. Simultaneous epitope and transcriptome measurement in single cells. *Nat Methods*. 2017;14:865–868. doi: 10.1038/nmeth.4380
60. Vanhersecke L, Bougouin A, Crombé A, Brunet M, Sofeu C, Parrens M, Pierron H, Bonhomme B, Lembege N, Rey C, et al. Standardized pathology screening of mature tertiary lymphoid structures in cancers. *Lab Invest*. 2023;103:100063. doi: 10.1016/j.labinv.2023.100063.
61. Sato Y, Silina K, van den Broek M, Hirahara K, Yanagita M. The roles of tertiary lymphoid structures in chronic diseases. *Nat Rev Nephrol*. 2023;19:525–537. doi: 10.1038/s41581-023-00706-z
62. Huang C, Wang W, Huang H, Jiang J, Ding Y, Li X, Ma J, Hou M, Pu X, Qian G, et al. Kawasaki disease: ubiquitin-specific protease 5 promotes endothelial inflammation via TNFα-mediated signaling. *Pediatr Res*. 2023;93:1883–1890. doi: 10.1038/s41390-022-02341-z
63. Huijbers MG, Lipka AF, Potman M, Hensbergen PJ, Titulaer MJ, Niks EH, van der Maarel SM, Klooster R, Verschuuren JJ. Antibodies to active zone protein ERC1 in Lambert–Eaton myasthenic syndrome. *Hum Immunol*. 2013;74:849–851. doi: 10.1016/j.humimm.2013.03.004
64. Wen X, Song G, Hu C, Pan J, Wu Z, Li L, Liu C, Tian X, Zhang F, Qian J, et al. Identification of novel serological autoantibodies in Takayasu arteritis

patients using HuProt arrays. *Mol Cell Proteomics*. 2021;20:100036. doi: 10.1074/mcp.RA120.002119
65. Wilson NR, Olm-Shipman AJ, Acevedo DS, Palaniyandi K, Hall EG, Kosa E, Stumpff KM, Smith GJ, Pitstick L, Liao EC, et al. SPECC1L deficiency results in increased adherens junction stability and reduced cranial neural crest cell delamination. *Sci Rep*. 2016;6:17735. doi: 10.1038/srep17735
66. Huang Y, Li J, Zhu X. Detection of anti-envoplakin and anti-periplakin autoantibodies by ELISA in patients with paraneoplastic pemphigus. *Arch Dermatol Res*. 2009;301:703–709. doi: 10.1007/s00403-008-0901-y
67. Al-Jassar C, Bernadó P, Chidgey M, Overduin M. Hinged plakin domains provide specialized degrees of articulation in envoplakin, periplakin and desmoplakin. *PLoS One*. 2013;8:e69767. doi: 10.1371/journal.pone.0069767
68. The Human Protein Atlas. Cell Line: PPL. Accessed February 28, 2026. https://www.proteinatlas.org/ENSG00000118898-PPL/cell+line
69. Siontis KC, Santangeli P, Muser D, Marchlinski FE, Zeppenfeld K, Hoogendoorn JC, Narasimhan C, Sauer WH, Zipse MM, Kapa S, et al. Outcomes associated with catheter ablation of ventricular tachycardia in patients with cardiac sarcoidosis. *JAMA Cardiol*. 2022;7:175–183. doi: 10.1001/jamacardio.2021.4738
70. Komatsu N, Takayanagi H. Mechanisms of joint destruction in rheumatoid arthritis: immune cell–fibroblast–bone interactions. *Nat Rev Rheumatol*. 2022;18:415–429. doi: 10.1038/s41584-022-00793-5
71. Krausgruber T, Redl A, Barreca D, Doberer K, Romanovskaia D, Dobnikar L, Guarini M, Unterluggauer L, Kleissl L, Atzmüller D, et al. Single-cell and spatial transcriptomics reveal aberrant lymphoid developmental programs driving granuloma formation. *Immunity*. 2023;56:289–306.e7. doi: 10.1016/j.immuni.2023.01.014
72. Liu J, Ma P, Lai L, Villanueva A, Koenig A, Bean GR, Bowles DE, Glass C, Watson M, Lavine KJ, et al. Transcriptional and immune landscape of cardiac sarcoidosis. *Circ Res*. 2022;131:654–669. doi: 10.1161/CIRCRESAHA.121.320449
73. Caforio ALP, Tona F, Bottaro S, Vinci A, Dequal G, Daliento L, Thiene G, Iliceto S. Clinical implications of anti-heart autoantibodies in myocarditis and dilated cardiomyopathy. *Autoimmunity*. 2008;41:35–45. doi: 10.1080/08916930701619235
74. Chatterjee D, Fatah M, Akdis D, Spears DA, Koopmann TT, Mittal K, Rafiq MA, Cattanach BM, Zhao Q, Healey JS, et al. An autoantibody identifies arrhythmogenic right ventricular cardiomyopathy and participates in its pathogenesis. *Eur Heart J*. 2018;39:3932–3944. doi: 10.1093/eurheartj/ehy567
75. Vereckei A, Katona G, Révész K, Vágó H, Müller V, Nagy B, Nagy P, Sepp R, Suvarna K. Cardiac sarcoidosis completely mimicking biventricular arrhythmogenic cardiomyopathy. *ESC Heart Fail*. 2022;9:4304–4314. doi: 10.1002/ehf2.14123
76. Elwazir M, Krause ML, Bois JP, Christopoulos G, Kendi AT, Cooper JRLT, Jouni H, Abouezzeddine OF, Chareonthaitawee P, Abdelshafee M, et al. Rituximab for the treatment of refractory cardiac sarcoidosis: a single-center experience. *J Card Fail*. 2022;28:247–258. doi: 10.1016/j.cardfail.2021.07.008
77. Furie R, Rovin BH, Houssiau F, Malvar A, Teng YKO, Contreras G, Amoura Z, Yu X, Mok C-C, Santiago MB, et al. Two-year, randomized, controlled trial of belimumab in lupus nephritis. *N Engl J Med*. 2020;383:1117–1128. doi: 10.1056/NEJMoa2001180
78. Cheng RK, Kittleson MM, Beavers CJ, Birnie DH, Blankstein R, Bravo PE, Gilotra NA, Judson MA, Patton KK, Rose-Bovino L; American Heart Association Heart Failure and Transplantation Committee of the Council on Clinical Cardiology, and Council on Cardiovascular and Stroke Nursing. Diagnosis and management of cardiac sarcoidosis: a scientific statement from the American Heart Association. *Circulation*. 2024;149:e1197–e1216. doi: 10.1161/CIR.0000000000001240
79. Nadelmann ER, Gorham JM, Reichart D, Delaughter DM, Wakimoto H, Lindberg EL, Litviňukova M, Maatz H, Curran JJ, Ischiu Gutierrez D, et al. Isolation of nuclei from mammalian cells and tissues for single-nucleus molecular profiling. *Curr Protoc*. 2021;1:e132. doi: 10.1002/cpz1.132
80. Fleming SJ, Chaffin MD, Arduini A, Akkad A-D, Banks E, Marioni JC, Philippakis AA, Ellinor PT, Babadi M. Unsupervised removal of systematic background noise from droplet-based single-cell experiments using CellBender. *Nat Methods*. 2023;20:1323–1335. doi: 10.1038/s41592-023-01943-7
81. Taliun D, Harris DN, Kessler MD, Carlson J, Szpiech ZA, Torres R, Taliun SAG, Corvelo A, Gogarten SM, Kang HM, et al; NHLBI Trans-Omics for Precision Medicine (TOPMed) Consortium. Sequencing of 53,831 diverse genomes from the NHLBI TOPMed Program. *Nature*. 2021;590:290–299. doi: 10.1038/s41586-021-03205-y
82. Kalantar KL, Carvalho T, de Bourcy CFA, Dimitrov B, Dingle G, Egger R, Han J, Holmes OB, Juan Y-F, King R, et al. IDseq: an open source cloud-based pipeline and analysis service for metagenomic pathogen detection and monitoring. *GigaScience*. 2020;9:giaa111. doi: 10.1093/gigascience/giaa111
83. Bernstein NJ, Fong NL, Lam I, Roy MA, Hendrickson DG, Kelley DR. Solo: doublet identification in single-cell RNA-Seq via semi-supervised deep learning. *Cell Syst*. 2020;11:95–101.e5. doi: 10.1016/j.cels.2020.05.010
84. van den Boogaart K, Tolosana-Delgado R, Bren M. compositions: Compositional Data Analysis. R package version 2.0-8. Published 2024. Accessed April 22, 2025. https://cran.r-project.org/web/packages/compositions/compositions.pdf
85. Jin S, Guerrero-Juarez CF, Zhang L, Chang I, Ramos R, Kuan C-H, Myung P, Plikus MV, Nie Q. Inference and analysis of cell–cell communication using CellChat. *Nat Commun*. 2021;12:1088. doi: 10.1038/s41467-021-21246-9
86. Mohan D, Wansley DL, Sie BM, Noon MS, Baer AN, Laserson U, Larman HB. PhIP-seq characterization of serum antibodies using oligonucleotide-encoded peptidomes. *Nat Protoc*. 2018;13:1958–1978. doi: 10.1038/s41596-018-0025-6
87. Hahsler M, Piekenbrock M, Doran D. dbscan: Fast Density-Based Clustering with *R*. *J Stat Soft*. 2019;91. doi: 10.18637/jss.v091.i01. http://www.jstatsoft.org/v91/i01